

Response to Review of HESSD-552-2015 by Anonymous Reviewer #1

Note: Original reviewer comments are in black and author's responses are in blue throughout. The changes in manuscript are in track change. The line numbers mentioned are according to the revised version of the manuscript

Major comments:

- (1) My main concern is that the manuscript does not present any new theory (and on top of that uses an approach (STICS) that in my opinion is misguided, despite the fact that it has been published).

Summary response: We thank R1 for the comments and firmly object the statement on 'misguidance' which appears to be potentially misleading particularly when a large part of the community have outright enthusiasm in developing analytical approaches for estimating terrestrial evapotranspiration (E) (or latent heat flux, λE) and sensible heat fluxes (H) to overcome the ambiguities associated with parameterizations of aerodynamic (g_A) and canopy surface conductances (g_C) (Kleidon et al., 2014; Matheny et al., 2014; Ershadi et al., 2015). Besides, we would like to clarify that the abbreviation for our model framework is "STIC" and not "STICS" as referred to by R1.

R1's claim is flawed because STIC (Surface Temperature Initiated Closure) introduced a novel analytical method to integrate radiometric surface temperature (T_R) into the Penman-Monteith model to overcome the limitations associated with empirical (uncertain) leaf-scale parameterizations of the aerodynamic and canopy surface conductances (g_A and g_C) which are not directly measurable either at the canopy-scale or at the large spatial grid-scale. To our knowledge, this research objective is unquestionably novel and the behavior of the analytically retrieved canopy-scale conductances as well as transpiration are compliant with the theory earlier postulated in the literatures (Jarvis and McNaughton, 1986; Monteith, 1995; Raupach, 1998). In addition to its simplicity, STIC has the capabilities for generating spatially explicit surface energy fluxes and independent of submodels for boundary layer developments.

The characteristic features of STIC are explicitly stated in section 2.1 (Theory) and 2.2 (State equations).

Detailed response: The most tangible accomplishment and uniqueness of STIC (STIC1.2) is the physical integration of land surface temperature (i.e., radiometric surface temperature, T_R) into a combined framework of the Penman-Monteith (PM) and Shuttleworth-Wallace (SW) model for simultaneously estimating E , H , g_A , g_C , surface moisture status, and E components (evaporation, E_E and transpiration, E_T). The intrinsic link between the PM-SW model and T_R emanates through the first-order dependence of the biophysical conductances (g_A and g_C) on the aerodynamic temperature (T_0) (through T_R) and soil moisture (through T_R). However, until now the explicit use of T_R in the PM-SW model was hindered due to the unavailability of any direct method to integrate T_R into these models, and, furthermore, due to the lack of physical models expressing biophysical states of vegetation as a function of T_R . Therefore, the majority of the E modeling approaches strongly rely on surface reflectance and meteorology; and thermal approaches require significant parameterization of land surface properties (e.g., g_A and g_C) which are very empirical in nature (Schulz and Beven, 2003; Prihodko et al., 2008; Bonan et al., 2014; Ershadi et al., 2015).

To bridge this gap, the STIC methodology was developed as a novel thermal-based biophysical scheme for directly estimating E over terrestrial ecosystems by leveraging the combined strength of T_R observations and physically-based models (Mallick et al., 2014; 2015). In addition to physically integrating T_R observations into a combined PM-SW framework, STIC1.2 also establishes of a feedback loop describing the relationship between T_R and E , coupled with canopy-atmosphere components relating E to aerodynamic temperature (T_0) and vapor pressure (e_0) (in STIC1.2). By integrating T_R with standard surface energy balance (SEB) theory and vegetation biophysical principles, STIC formulates multiple state equations in order to eliminate the need of exogenous parametric submodels for the surface and aerodynamic conductances, aerodynamic temperatures, and land-atmosphere coupling. Instead these 'internal states' are numerically retrieved. Originally designed for application to thermal remote sensing data from Earth observation sensors, the STIC framework exploits observations of T_R , radiative, and meteorological variables including net radiation (R_N), ground heat flux (G), air temperature (T_A), relative humidity (R_H) or vapor pressure (e_A) at a reference level above the surface, and can be applied over any ecosystem, provided the necessary input variables are available.

(2) STICs is misguided because it ends up with an aerodynamic conductance that does not depend on wind speed.

Summary response: R1 claims that STIC is misguided due to two reasons. According to R1, the first reason should be that aerodynamic conductance does not depend on wind speed (u). **It should be noted that, in one of the hallmark papers by Choudhury and Monteith (1986), it is clearly stated that 'aerodynamic conductance determined by wind speed and roughness is assumed to be unaffected by buoyancy'. Strictly, the aerodynamic conductance should be replaced by a term which accounts for radiative as well as convective heat transfer**. Although incorporation of u data has almost become a dogma (Foken, 2006) in the field of land surface energy balance modelling, there are several widely accepted evapotranspiration estimation approaches that do not incorporate W_s , for example, maximum entropy production approach (Kleidon et al., 2014), evaporative fraction approach (Jiang and Islam, 2001; Batra et al., 2006), complementary relationship approach (Venturini et al., 2008) etc.

A table is included in the Appendix (Table A2) which describes the fundamental differences in g_A modeling between the conventional approaches and STIC.

Detailed response: Given the importance of g_A for evapotranspiration (E) estimates there are overriding cases for getting this 'right' in the surface energy balance models (Prihodko et al., 2008; Hong et al., 2010; Gibson et al., 2011; Holwerda et al., 2012; Gokmen et al., 2012; Morillas et al., 2013). However, if the empirical g_A models currently provide accurate estimates of E for the wrong reasons then this status quo has to be questioned, especially as errors like this might become important when predicting E under future boundary conditions. Furthermore, it is not obvious that W_s -based models currently provide accurate estimates of g_A , in particular at the grid-scale (e.g., 1 km and above) where bundles of site specific parameters are required (which cannot be measured).

We would like to bring forward the following arguments concerning W_s -based g_A estimation.

- (a) As highlighted in several studies (Monteith and Unsworth, 2008; Holwerda et al., 2012), the momentum transfer equation for g_A estimation based on the Monin-Obukhov Similarity Theory (MOST) only holds for an extended, uniform, and flat surface (Foken, 2006). MOST tends to fail over rough surfaces due to breakdown of the similarity relationships for heat and water vapour transfer in the roughness sub-layer, which results in an underestimation of the 'true' g_A by a factor 1-3 (Thom et al., 1975; Chen and Schwerdtfeger, 1988; Simpson et al., 1998; Holwerda et al., 2012). Despite some of the boundary layer studies based on parameterized friction velocity (u^*) demonstrated the validity of MOST (subjected to tuning and calibration) (Harman and Finnigan, 2007; 2008), a considerable number of studies have casted scepticism on the validity of u^* parameterization in the framework of MOST (Foken, 2006; Holwerda et al., 2012; van Dijk et al., 2015). **It is imperative to mention that g_A is one of the main anchors in the PM-SW model because it not only appears in the numerator and denominator of these models, g_A also provides feedback to g_C , aerodynamic temperature, and vapor pressure (seminal paper of Jarvis and McNaughton, 1986).** Therefore, the estimates of E and interception evaporation (E_i) in the PM-SW framework are robustly sensitive to parameterization of g_A and stable E estimates might be possible if g_A estimation is unambiguous (Holwerda et al., 2012; van Dijk et al., 2015). Consequently, our aim was to find analytical solution of g_A , and through algebraic reorganization of surface energy balance equation we are able to do so. **Given the lack of consensus in the community on the 'true' g_A , we treat STIC1.2 derived non-parametric g_A to be the aerodynamic conductance that satisfies the PM-SW equation for estimating evaporative fluxes.**
- (b) In the state-of-art E modeling, the parametric g_A sub-models are stand alone and empirical, and do not provide any feedback to the canopy (or surface) conductances (g_C), aerodynamic temperature (T_0), and aerodynamic vapor pressure deficit (D_0). However, g_A is an internal state that provides physical feedback to E and H by influencing T_0 , D_0 , and g_C . Large g_A indicates **small gradients of vapor pressure deficit between the air and canopy boundary layer** and hence strong coupling between canopy and atmosphere (Jarvis and McNaughton, 1986). **These biophysical interactions are entirely overlooked in the land surface parameterizations of g_A (but are included in STIC).** **STIC1.2 consists of a feedback describing the relationship between T_R and E, coupled with canopy-atmosphere components relating E to T_0 and e_0 . The equations are explicitly stated in the Appendix (A2) (eq. A9 to A17) of the manuscript and the detailed descriptions are in L764 to L808.**
- (c) **Additional challenges** in grid-scale or spatial-scale g_A estimation are the **requirements of numerous site specific parameters** (e.g., vegetation height, measurement height, vegetation roughness, leaf size, soil roughness) and **coefficients** needed to correct the atmospheric stability conditions (Raupach, 1998). **These informations are required to fulfil the set of assumption established around 1960's**, that can and should be questioned by the community if we want to make science advance in the field of surface energy balance modeling.
- (d) The enhanced errors in E estimates in water-limited regions due to uncertain g_A parameterization (Gibson et al., 2011; Timmermans et al., 2013; Morillas et al., 2013; Castellvi et al., 2016) and repeated adjustment of different vegetation as well as soil parameters in the conductance equations to obtain a better E validation (Gokmen et al., 2012) questions the validity of wind driven non-stationary g_A parameterizations. **It solicits for revisiting the state-of-art g_A parameterizations and rethinking to develop a calibration independent g_A modelling framework.**

(e) The credibility of STIC1.2 g_A estimates is shown in the figures (Fig. 1 and Fig. 2). While Fig. 1a in the manuscript illustrates the differences in the g_A magnitude between forest and pasture, Fig. 2a displays an independent comparison of STIC- g_A versus u^* -based g_A . Fig. 2e and 2f showed that T_R , vapor pressure deficit (D_A), and net available energy (ϕ) (difference between net radiation, R_N and ground heat flux, G) can explain 42% to 83% variability of the u^* -based g_A . **These correlations and scatterplots between u^* -based g_A with radiative and meteorological variables clearly emphasize the explanatory power of these variables to characterize wind-driven g_A and the appropriateness of deriving an analytical g_A without wind speed. This also supports the findings of Villani et al. (2003) which stated that during unstable surface layer conditions the major source of net available energy is located at the canopy top and drives the convective motion in the layers above. Hence, the value of g_A is not only controlled by wind speed as advocated by R1.**

(3) STICs is misguided because it introduces a soil moisture stress term that only depends on atmospheric variables.

Response: R1's claim is not substantiated because the water stress factor was estimated by combining the radiometric surface temperature (T_R) with air temperature (T_A), dewpoint temperature (T_D), and near surface dewpoint temperature (T_{SD}) as explained in Mallick et al. (2015).

The methodology is explained in section 2.1 (L205 to L229), section 2.2, and in the Appendix (A2) of the revised manuscript. In STIC1.2, T_{SD} was estimated in an iterative mode to establish a feedback between the water stress, T_R , T_{SD} , and evapotranspiration (explained in Appendix A2).

(4) The paper then uses Amazonian micrometeorological data to compare a range of g_A and g_C terms. No measurements of g_C are used to provide verification.

Response: The reasons are explicitly stated in section 2.4 (L337 to L343).

This exercise could not be performed as direct canopy-scale g_C observations are not possible with current measurement techniques. Although leaf-scale measurements of g_C are relatively straightforward, these values are not comparable to values retrieved at the canopy-scale. However, assuming u^* -based g_A as baseline aerodynamic conductance, we had estimated canopy-scale g_C by inverting the PM equation (g_{C-INV}) to evaluate g_{C-STIC} . The comparison between g_{C-STIC} and g_{C-INV} over forest and pasture is illustrated in Fig. 3a, and the results are discussed in L305 to L315 of the earlier manuscript (L425 to L434 of the revised manuscript).

(5) A large number of plots are then presented where STICS variables are plotted against meteorological variables in a host of different ways. I am not surprised to see that these dependencies exist as all of them are intrinsic to the model. Also, because all of them are interdependent I am not sure how much realism there ultimately is in the findings.

Summary response: We do not agree with this statement of R1. Firstly, comparing different g_A estimates, linking the wind driven g_A estimates with some independent variables (Fig. 2), and STIC driven g_A estimates with some interdependent variables (Fig. 6 to Fig. 8) is not a matter of choice, but a necessity, as it evident to any reader. The same is applicable to Fig.

6 to Fig. 8 for g_C . Secondly, despite the transpiration and evaporation estimates are interdependent with g_C and g_A (as shown in Fig. 6 to Fig. 8); the figures reflect the credibility of the conductances as well as transpiration estimates by realistically capturing the hysteretic behavior between biophysical conductances and water vapor fluxes which is frequently observed in natural ecosystems (Zhang et al., 2014, Renner et al., 2016). Fig. 8 (a, b) also affirms that the conductance-transpiration-vapor pressure deficit relationships are compliant with the stomatal feedback-response theory earlier postulated from observational evidences (Monteith, 1995).

Necessary explanations are included in the revised manuscript (L662 to L672)

Detailed response: Fig. 2 illustrates the diagnostic potential of thermal (T_R), radiative (ϕ), and meteorological (D_A) variables to explain the wind driven g_A variability (wind driven g_A is independently estimated).

Fig. 6 and 7 explains the ‘hysteresis’ between transpiration and conductances which shows the degree of hysteresis was larger in the dry season than in the wet season. These results are compliant with the theories earlier postulated from observations that the magnitude of hysteresis depends on the radiation-vapor pressure deficit lag, while the soil moisture availability is a key factor modulating the hysteretic transpiration-vapor pressure deficit relation as soil moisture declines (Zhang et al., 2014; O’Grady et al., 1999; Jarvis and McNaughton, 1986). **This shows that despite independent of any predefined hysteretic function, the interdependent conductance-transpiration hysteresis is still captured in STIC1.2 (which are generally observed in natural ecosystems).**

Fig. 8 (a and b) confirms the ‘stomatal feedback-response’ hypothesis as postulated by Lt. John Monteith (Monteith, 1995), which states that a decrease in stomatal conductance with increasing vapor pressure deficit is caused by a direct increase in transpiration (Monteith, 1995) and stomata responds to the changes in the air humidity by sensing transpiration, rather than vapor pressure deficit. This feedback mechanism is found because of the influence of vapor pressure deficit on both stomatal conductance and transpiration, which in turn changes vapor pressure deficit by influencing the air humidity (Monteith, 1995).

Fig. 8c shows the complex interaction between g_C , radiometric surface temperature (T_R) and vapor pressure deficit (D_A). This also answers why different parametric g_C models produce divergent results.

Fig. 8d emphasizes the behavior of g_A according to existing theory that under extremely high atmospheric turbulence (i.e., high g_A), a close coupling exists between the surface and the atmosphere, which causes T_R and T_A to converge (i.e., $T_R - T_A \rightarrow 0$).

- (6) Furthermore STICS assumes that $T_0 = T_R$ and yet the manuscript does not mention the potential implications of this assumption, nor the fact that considerable errors can be made when measuring T_R .

Summary response: This comment by R1 is incorrect. In STIC1.2, T_0 is analytically estimated by integrating T_R into a combined PM-SW framework. The analytical expression of T_0 is dependent on M and the estimation of M is based on T_R as described in the Appendix (A2) of the current manuscript. T_0 is a function of T_R in STIC and they are not assumed equal (section 2.2, L286 to L290). To further address R1's point on the assumption that $T_0=T_R$, we show here an intercomparison of retrieved T_0 versus T_R for forest and pasture (figure below). This indicates the distinct difference of the retrieved T_0 from T_R for the two different biomes, which proves that R1's claim to be invalid.

We have included this figure of T_0 versus T_R and in the Appendix of revised manuscript (Fig. A2). We have addressed this point explicitly (i.e., $T_0 \neq T_R$) in section 2.2 of the manuscript.

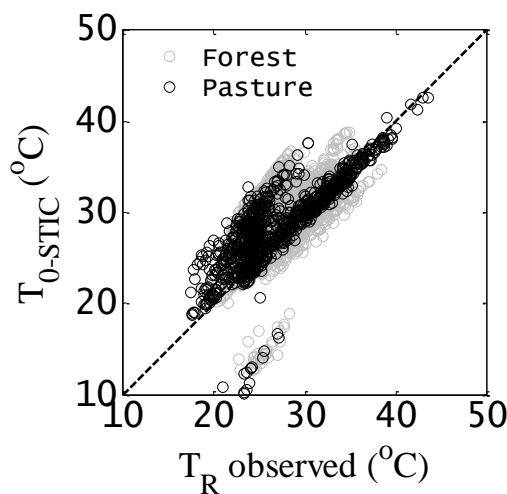


Figure: Aerodynamic temperature obtained from STIC1.2 (T_{0-STIC}) versus radiometric surface temperature (T_R) over two different biomes in the Amazon basin. The regression equation of line of best fit is $T_{0-STIC} = 0.67(\pm 0.10)T_R + 10.59(\pm 2.79)$ with $r = 0.65$

Detailed response: One of the core objectives of the original STIC formulation was to physically integrate T_R into the PM model to constrain the conductances. **This is done by estimating an aggregated surface moisture availability (or water stress factor) which is an emphatic function of T_R .** A detailed description of the STIC state equations is given in Mallick et al. (2015) and novel part of STIC1.2 is described in the Appendix (A2) of the revised manuscript.

(7) In the end I feel I have learned little new and what has been presented is tentative and therefore potentially misleading. This is underlined by sentences (line 325-329) such as "The evaluation of the conductances and surface energy fluxes indicates some efficacy for the STIC derived fluxes and conductance estimates As a result we feel some justification for exploring the canopy-scale biophysical controls on ET and EE generated through the STIC framework".

Response: We do not agree with the reviewer's impression. The major novelties of the present manuscript are as follows:

The bafflement about estimating λE originates from complex supply-demand interactions, where net radiation and soil moisture represents the supply and the atmospheric vapor pressure deficit represents the demand. This supply-demand interaction accelerates the biophysical feedbacks in λE and understanding these biophysical feedbacks is necessary to

assess the terrestrial biosphere response to water availability. This is now explicitly mentioned in L98 to L102 (also L175 to L188, section 2.1 and section 2.2) of the revised manuscript.

In this context, the entire manuscript is about understanding the canopy-scale biophysical controls on transpiration and evaporation over the Amazon basin. The two critical biophysical state variables (i.e., g_A and g_C) in the PM equation are the unobserved components which cannot be measured directly. Therefore, we explored the radiative (net radiation and ground heat flux), meteorological (air temperature and relative humidity), and thermal (radiometric surface temperature) information, and developed the STIC framework to analytically estimate these variables in an internally consistent manner (as described in the manuscript). However, before understanding the controls of g_A and g_C on transpiration and evaporation, some indirect evaluation of these two biophysical states was necessary. The sentence is changed as "The evaluation of the conductances and surface energy fluxes indicates some efficacy for the STIC derived fluxes and conductance estimates which represent a weighted average of these variables over the source area around EC tower".

Detailed comments:

Line 81-82: "An intensification of the Amazon hydrological cycle was observed in the past two decades characterised by increased temperatures and more frequent droughts and floods" How are increased air (?) temperatures directly linked to hydrological cycle? If it is surface temperatures then say this, but this would mean a decreased ET (hence the floods?)

Response: Necessary corrections are made in L84 to L85.

Line 86: "the Amazon forest may become an increasing carbon source". Should this be "increasingly become a net source of carbon?"

Response: Necessary corrections are made in L88 to L91.

Line 97-104: I disagree with the final point made in this section: GC does not include the conductance relating to bare soil. If you would have called it the surface conductance instead and defined it via the PM Big leaf equation I would have agreed.

Response: We do not agree and texts are included in L110 to L112 and L236 to L239.

For a dense canopy, g_C in the PM equation represents the canopy surface conductance. Although it is not equal to the canopy stomatal conductance, it contains integrated information of the stomata. For a heterogeneous landscape, g_C in the PM equation is an aggregated surface conductance containing information of canopy and soil.

Lines 111-126 are stating the obvious. Where is this going?

Response: These sentences (L127 to L142 in the revised manuscript), and explained the unresolved challenges and problems associated with g_A and g_C parameterisations. **If these are obvious, R1's previous claims on g_A appear to be unfounded.**

These statements are needed to recognize the need of a non-parametric g_A and g_C modeling framework.

Line 136: Why is the partitioning between soil evaporation and transpiration deemed so important in the Amazon? Soil evaporation must only make up a small part of total ET. Will this soil term affect flooding, atmospheric circulation etc. I highly doubt this.

Response: We intended to address ‘evaporation’, not ‘soil evaporation’ (L152 in the revised manuscript). In the Amazon forest, although the soil evaporation has negligible contribution, it is the interception evaporation that has substantial contribution in the total evaporative fluxes, and, therefore the partitioning of ‘evaporation (λE_E)’ and ‘transpiration (λE_T)’ is significant.

Line 141-143: “Given the persistent risk of deforestation, the ecophysiological changes of different plant functional types (PFTs) are expected to be reflected in g_A and g_C and EE and ET”. I really do not understand what is meant by this sentence.

Response: This is now L157 to L161 and necessary changes are incorporated.

The persistent risk of deforestation is likely to alter the radiation interception, surface temperature, surface moisture, associated meteorological conditions, and vegetation biophysical states of different plant functional types (PFTs). Conversion from forest to pasture is expected to change the g_C/g_A ratio of these ecosystems and impact the evapotranspiration components.

Line 154-157: The surface temperature is already implicit in the PM equation as it combines the energy balance with bulk transfer equations.

Response: The surface temperature (T_R) was eliminated from the derivation of the PM equation by expressing the slope of the saturation vapor pressure at ambient air temperature. However, in the seminal paper titled ‘Evaporation and Surface Temperature’ (Monteith, 1981), Lt. John Monteith described the role of leaf temperature in constraining the biophysical conductances. Although T_R is implicit in the net radiation (R_n), which appears in the numerator of the PM equation, it may be noted that R_n has a relatively weak dependence on T_R (compared to T_R sensitivities of soil moisture and E). No universally agreed formulation is available that physically constrains g_A and g_C by using T_R . Development of STIC is based on the assumption that the intrinsic link between the PM-SW model and T_R emanates through the first-order dependence of the biophysical conductances on aerodynamic temperature (T_0) and soil moisture (through T_R). Hence, the conductances are explicitly constrained by using T_R information as described in the manuscript.

Detailed explanations are given in L213 to L229 and in section 2.2.

Line 179-181: “The retrieval of g_A , g_C , and E are based on finding a ‘closure’ of the PM equation using the STIC framework”. In my opinion, the PM is already closed, see my point above. It calculates ET from $R_n - G$, and H is implicitly in there. Please study books such as those by Hamlyn Jones to see how PM equation is derived.

Response: The PM equation is ‘closed’ upon the availability of canopy-scale measurements of the two unobserved biophysical conductances (g_A and g_C) and if we assume the empirical models of g_A and g_C to be reliable. However, neither g_A nor g_C can be measured at the canopy-scale or at larger spatial scales. Furthermore, as shown by several recent studies (Matheny et al., 2014; van Dijk et al., 2015) a most appropriate or correct g_A - g_C model is

currently not available. This implies that a true ‘closure’ of the PM equation is only possible upon analytical estimation of the conductances. Necessary explanations are given in L242 to L248.

Line 184: This should be ‘radiative temperature’.

Response: Necessary correction is made (L210).

Line 203: You have now tacitly assumed that $T_0 = T_R$. There is a host of literature references that will tell you otherwise.

Response: The explanation is already provided above; there is no assumption on the equality between T_R and T_0 . We have addressed this point explicitly (i.e., $T_0 \neq T_R$) in section 2.2 of the manuscript.

Line 204-205: PM equation is already closed. This assumption of energy balance closure is implicit in its derivation. But maybe I do not understand what you mean by this statement.

Response: As mentioned earlier, the PM equation is closed if measurements of the two unobserved biophysical conductances (g_A and g_C) are available. However, g_A and g_C cannot be directly measured at the canopy-scale and there is no universally agreed g_A and g_C model. By the term ‘closure’, we mean actual ‘closure’ of the PM equation by finding analytical solutions of g_A and g_C . This was done by solving ‘n’ equations and ‘n’ unknowns as described in equation 2 to 5 in the manuscript. The derivation of these equations are explained in the Appendix (A1) of the revised manuscript.

Line 225-227: “The estimates of EE in the current method consists of aggregated contribution from both interception and soil evaporation, and no further attempt is made to separate these two components”. This is a considerable weakness in the approach seeing leaf area index and hence interception is so large for large parts of the Amazon and soil evaporation will be negligible. You are making this point yourself a few sentences later (line 232) Also: these two types of evaporation fluxes take place at very different source heights, so their GA will be very different, further weakening your approach.

Response: We do not agree. This is not a considerable weakness, but a fact which is clearly stated instead of withholding it. At the outset, the biophysical controls on evaporation and transpiration are mentioned, and no claim is made on understanding soil evaporation, interception evaporation etc.

We agree that different g_A exists for soil-canopy, sun-shade, and dry-wet conditions; which is currently integrated into a lumped g_A (given the big-leaf nature of STIC). From the big-leaf perspective, it is generally assumed that the aerodynamic conductance of water vapor and heat are equal (Raupach, 1998). However, for obtaining partitioned aerodynamic conductances, explicit partitioning of evapotranspiration is needed, which is beyond the scope of the current manuscript. This is mentioned in L315 to L320 (section 2.3) of the revised manuscript.

Line 285: “The conductances showed a marked diurnal variation expressing their overall dependence on net radiation, vapor pressure deficit, and surface

temperature". What conductance are you referring to here? g_A or g_C ? Or both? Note that g_A generally does not depend on net radiation or VPD etc., although it does in STICS.

Response: Here, we are referring to both g_A and g_C as clearly stated in Fig. 1 and the related descriptions as stated in [L399 to L408](#).

The role of g_A is associated with the role of convection (Choudhury and Monteith, 1986) according to the surface energy balance principle as follows.

Neglecting horizontal advection and energy storage, the surface energy balance equation is written as follows:

$$\phi = \lambda E + H \quad (1)$$

Where $\phi \cong R_N - G$, with R_N being net radiation, and G being the conductive surface heat flux or ground heat flux, H is the sensible heat flux and λE is the latent heat flux.

The sensible and latent heat flux can be expressed in the form of aerodynamic transfer equations (Boegh et al., 2002; Boegh and Soegaard, 2004) as follows:

$$H = \rho c_P g_A (T_o - T_A) \quad (2)$$

$$\lambda E = \frac{\rho c_P}{\gamma} g_A (e_o - e_A) = \frac{\rho c_P}{\gamma} g_C (e_o^* - e_o) \quad (3)$$

Where T_A is the air temperature at the reference height (z_R), e_A is the atmospheric vapor pressure (hPa) at the level at which T_A is measured, e_o and T_o are the atmospheric vapor pressure and air temperature at the source/sink height, or at the so-called roughness length (z_o), where wind speed is zero. They represent the vapor pressure and temperature of the quasi-laminar boundary layer in the immediate vicinity of the surface level (Fig. A1), and T_o can be obtained by extrapolating the logarithmic profile of T_A down to z_o . e_o^* is the saturation vapor pressure at T_o (hPa).

By combining eq. 1, 2, and 3 and solving for g_A , we get

$$g_A = \frac{\phi}{\rho c_P \left[(T_o - T_A) + \left(\frac{e_o - e_A}{\gamma} \right) \right]} \quad (4)$$

Equation 4 clearly portrays the dependency of g_A on net available energy and vapor pressure.

Given R1's disposition on the wind speed dependent empirical g_A models based on the Monin-Obukhov Similarity Theory (MOST), it is important to mention that the Monin-Obukhov Length (L) is a function of evapotranspiration (E) (Brutsaert, 1982), and E is strongly dependent on the net available energy as well as vapor pressure deficit. The functions below describes the dependence of g_A on net available energy (ϕ) (= net radiation – ground heat flux) and vapor pressure deficit in addition to $T_o - T_A$, despite g_A being generally estimated from wind speed information.

$$g_A = f\{L\} \quad (5)$$

$$L = \frac{u^* \rho C_p T_A}{g(H + 0.61 C_p T_A E)} \quad (6)$$

$$u^* = f\{L, E, \text{specific humidity gradient, wind speed}\} \quad (7)$$

$$E = f\{R_N, D_A, \text{soil moisture, } T_R\} \quad (8)$$

Here u^* is the friction velocity (m s^{-1}), ρ is the air density (kg m^{-3}), c_p is the specific heat of air ($1004 \text{ J kg}^{-1} \text{ K}^{-1}$), T_A is the air temperature (K), D_A is the vapor pressure deficit (hPa). Rest all the variables are explained earlier.

According to equations 5 to 8, the dependence of g_A on net radiation and D_A is obvious. Wind is generated as a result of the differences in atmospheric pressure which is a result of uneven surface radiative heating. Therefore, the aerodynamic conductance (and wind as well) is an effect of net radiative heating and therefore, there should be a physical relationship between these two.

Necessary explanations are given in Table (A2).

Response to Review of HESSD-552-2015 by Anonymous Reviewer #2

This manuscript describes a study that infers stomatal and aerodynamic conductances from eddy flux observations. I think in general, this study is innovative and presents novel material, so that in principle it should be published. I hesitate recommendation for publication mostly because I am not entirely convinced by the approach and I feel that this needs revision. Hence, I recommend major revisions, although I do not think that it necessarily involves a lot of work to address the points below.

Response: We thank R2 for the encouraging comments and for appreciating the novelty of the aerodynamic and canopy conductance (g_A and g_C) retrieval to assess their controls on evaporation and transpiration. We appreciate the valuable suggestions which will further improve the manuscript.

Major points:

- (1) My major problem with the manuscript is that I do not understand the approach, so that it is difficult to assess its plausibility. While the main equations are provided in the manuscript (eqn. 2-5), there is no more description on where these equations come from, except for references to prior papers by the authors. I think it is necessary to at least provide a description at a qualitative level where these equations come from.

Response: We agree and included the detailed derivations of the 'state equations' (eqn. 2 to 5) in the Appendix (A1) of the revised manuscript.

- (2) The point where I really got confused is that eqn. 5 uses the Priestley-Taylor coefficient, which is an empirical coefficient in an evaporation equation that is rather different from the Penman Monteith equation. Where does this coefficient suddenly come from? I find this quite confusing, and it needs at least a minimum of explanation as it is not obvious.

Response: Good point indeed and we apologize for the confusion. This description is made explicit in the revised version of the manuscript ([L279 to L283](#)).

From the derivation of the [equation S10 \(described in Supplement in the manuscript\)](#), it is apparent that the Priestley-Taylor coefficient (α) appeared due to the use of the Advection-Aridity hypothesis for deriving the state equation of the evaporative fraction. However, instead of assuming α as a 'fixed parameter', we have developed a physical equation of α (eqn. A15 in the manuscript) and numerically estimated α as a 'variable'. **The derivation of the equation for α is described in the [Appendix A2 of the manuscript in L780 to L782](#).**

- (3) What I also do not understand is why an iterative scheme is needed.

Response: The analytical solution to the 'state' equations (eqn. 2 – 5 in the manuscript) have four accompanying unknowns; M (surface moisture availability), e_0 (vapor pressure at the source/sink height), e_0^* (saturation vapor pressure at the source/sink height), and α , and as a result there are 4 equations with 8 unknowns. Consequently an iterative solution is needed

to determine the four unknown variables as stated in [L265 to L271 of the revised manuscript and described in the Appendix A2](#).

(4) Can't one simply use the observations and use a simple partitioning based on the Bowen ratio?

Response: Here we intended to partition evapotranspiration into component water fluxes. Although the Bowen ratio (Bowen, 1926) is an energy partitioning ratio to understand the relative apportioning between sensible and latent heat flux, it is not relevant for the latent heat flux partitioning into transpiration and evaporation. In this context an aggregated surface moisture availability (or water stress factor) is a better metric for dry-wet latent heat flux partitioning and we used the retrieved surface moisture availability (M) for partitioning of the latent heat flux.

(5) It would be good to describe what the differences and similarities are to previous approaches. As the authors propose a new approach, they should provide a better description that is easier to follow of what is being done.

Response: We assume R2 is intending to the differences of STIC with other approaches that earlier attempted to understand the biophysical controls of evapotranspiration, which is described in [Table \(A2\)](#).

If R2 is intending the differences between STIC1.2 with other previous STIC versions, we included [Table \(A1\)](#) in the appendix to describe the fundamental differences between STIC1.0, STIC1.1, and STIC1.2.

Minor points:

- The authors refer to λE as evaporation, which, technically speaking, is the latent heat flux, not evaporation.

Response: Necessary corrections are made ([L37 to L38, L106 to L107](#)) in the revised manuscript.

- Abstract: dry and wet conditions λE_T , do you mean conditions in which water is not limiting vs. limiting, or precipitation vs. radiation driven conditions?

Response: It is the precipitation vs. radiation driven conditions and we have clarified this in the abstract ([L47 to L52](#)) of the revised manuscript.

- Biophysical control of λE_T should be briefly explained by what this means.

Response: At large g_A/g_C , the vapor pressure deficit close to the canopy source/sink height (D_0) approximates the atmospheric vapor pressure deficit (D_A) due to aerodynamic mixing and/or low transpiration. This results in a strong canopy-atmosphere coupling and such condition is prevalent under soil moisture deficient conditions. On the contrary, large g_C influences the gradients of vapor pressure deficit just above the canopy, such that D_0 tend towards zero and thus remains different from D_A (Jarvis and McNaughton, 1986). This

situation reflects a weak canopy-atmosphere coupling and such situation prevails under predominantly wet conditions and/or poor aerodynamic mixing due to wetness induced low aerodynamic roughness.

We have included this description in the introduction ([L112 to L120](#)) of the revised manuscript. Additionally, [section 2.5](#) also described the details about biophysical controls.

- Line 145: I wonder why approaches that directly link stomatal conductance to photosynthesis are not mentioned, such as Ball-Berry?

Response: We have included references to photosynthesis-dependent stomatal conductance models in the revised manuscript ([L162 to L163](#)).

- Line 194: Where do these “state equations” come from? Referring to previously published work is fine for derivations, but the description should still mention what the concepts are that are behind these equations.

Response: We have included a detailed description of the derivation of the ‘state equations’ in the [Appendix \(A1\)](#) of the revised manuscript.

- A table of variables would help.

Response: A table of variables has been included (Table 1).

- Line 238: I think the authors assume that the conductances to momentum, sensible and latent heat are identical. If this is the case, it should be mentioned, as there are also approaches to surface exchange that do not treat them as being identical.

Response: Yes, the conductances of momentum for the sensible and latent heat flux are assumed identical as mentioned in the revised manuscript ([L329 to L330](#)).

- Line 331: As the typical readers of HESS are not micrometeorologists, it would be useful to explain the decoupling coefficient in some more detail. This will help to interpret the following results.

Response: A detailed description of the decoupling coefficient is now included in [section 2.5](#). The decoupling coefficient or ‘Omega’ (Ω) is a dimensionless coefficient ranging from 0.0 to 1.0 (Jarvis and McNaughton, 1986) and considered as an index of the degree of stomatal control on transpiration. The equation of Ω is as follows:

$$\Omega = \frac{\frac{s}{\gamma} + 1}{\frac{s}{\gamma} + 1 + \frac{g_A}{g_c}}$$

Introducing Ω in the Penman-Monteith (PM) equation for λE results in:

$$\lambda E = \Omega \lambda E_{eq} + (1 - \Omega) \lambda E_{imp}$$
$$\lambda E_{eq} = \frac{s \phi}{s + \gamma}$$

$$\lambda E_{imp} = \frac{\rho c_P}{\gamma} g_C D_A$$

Where, λE_{eq} is the equilibrium evapotranspiration, which depends only on the net available energy and would be obtained over an extensive surface of uniform moisture availability (Jarvis and McNaughton, 1986; Kumagai et al., 2004). λE_{imp} is the imposed evapotranspiration, which is ‘imposed’ by the atmosphere on the vegetation surface through the effects of vapor pressure deficit (triggered under limited soil moisture availability) and evapotranspiration is proportional to g_C .

When the g_C/g_A ratio is very small (i.e., water stressed conditions), stomata principally control the water loss and a change in g_C will result in a nearly proportional change in transpiration. In this case the Ω value approaches zero, and vegetation is believed to be fully coupled to the atmosphere. In contrast, for a high g_C/g_A ratio (i.e., water unstressed conditions), changes in g_C will have little effect on the transpiration rate, and transpiration is predominantly controlled by the net available radiative energy. In this case the Ω value approaches unity, and vegetation is considered to be poorly coupled to the atmosphere.

- Line 422: To what extent could these discrepancies between how conductances are derived also relate to actual differences in the conductances for momentum vs. heat?

Response: This is indeed a good point addressed by R2 (although beyond the scope of this manuscript) and is clarified in the revised manuscript ([L537 to L546](#)).

- Line 498: The authors should stick to the same ratio g_A/g_C for easier interpretation.

Response: In the entire manuscript we maintain g_C/g_A ratio for easier interpretation, uniformity and also for the clarity to the reader.

Additional references:

Batra, N., Islam, S., Venturini, V., Bisht, G., and Jiang, L.: Estimation and comparison of evapotranspiration from MODIS and AVHRR sensors for clear sky days over the southern great plains, *Remote Sens. Environ.*, 103, 1–15, 2006.

Brutsaert, W.: *Evaporation Into the Atmosphere*, Reidel Pub. Comp., Dordrecht, Holland, 299 pp, 1982.

Castellví, F., Cammalleri, C., Ciraolo, G., Maltese, A. and Rossi, F.: Daytime sensible heat flux estimation over heterogeneous surfaces using multitemporal land-surface temperature observations, *Water Resour. Res.*, doi:10.1002/2015WR017587, 2016 (in press).

Gokmen, M., et al.: Integration of soil moisture in SEBS for improving evapotranspiration estimation under water stress conditions, *Remote Sens. Environ.*, 121, 261–274, 2012.

Harman, I.N., Finnigan, J.J.: Scalar concentration profiles in the canopy and roughness sublayer, *Bound. Layer Meteorol.* 129 (3), 323–351, 2008.

Harman, I.N., Finnigan, J.J., 2007. A simple unified theory for flow in the canopy and roughness sublayer. *Bound.-Layer Meteorol.* 123 (2), 339–363.

- Hong, J. and Kim, J.: Numerical study of surface energy partitioning on the Tibetan plateau: comparative analysis of two biosphere models, *Biogeosciences*, 7, 557-568, doi:10.5194/bg-7-557-2010, 2010.
- Jiang, L., and Islam, S.: Estimation of surface evaporation map over Southern Great Plains using remote sensing data, *Water Resour. Res.*, 37 (2), 329–340, 2001.
- Kleidon, A., Renner, M., and Porada, P.: Estimates of the climatological land surface energy and water balance derived from maximum convective power, *Hydrol. Earth Syst. Sci.*, 18, 2201-2218, 2014.
- Morillas, L., García, M., Nieto, H., Villagarcia, L., Sandholt, I., Gonzalez-Dugo, M.P., Zarco-Tejada, P.J., Domingo, F.: Using radiometric surface temperature for energy flux estimation in Mediterranean drylands from a two-source perspective, *Remote Sens. Environ.*, 136, 234 – 246, 2013.
- Prihodko, L., Denning, A.S., Hanan, N.P., Baker, I.T., and Davis, K.: Sensitivity, uncertainty and time dependence of parameters in a complex land surface model, *Agric. For. Meteorol.*, 148 (2), 268–287, 2008.
- Schulz, K., Beven, K.J.: Data-supported robust parameterisations in land surface-atmosphere flux predictions: towards a top–down approach, *Hydrol. Process.* 17, 2259–2277, 2003.
- Timmermans, J., Su, Z., van der Tol, C., Verhoef, A., and Verhoef, W.: Quantifying the uncertainty in estimates of surface–atmosphere fluxes through joint evaluation of the SEBS and SCOPE models, *Hydrol. Earth Syst. Sci.*, 17, 1561-1573, doi:10.5194/hess-17-1561-2013, 2013.

Canopy-scale biophysical controls of transpiration and evaporation in the Amazon Basin

Kaniska Mallick¹, Ivonne Trebs¹, Eva Boegh², Laura Giustarini¹, Martin Schlerf¹, Darren T. Drewry³, Lucien Hoffmann¹, Celso von Randow⁴, Bart Kruijt⁵, Alessandro Araùjo⁶, Scott Saleska⁷, James R. Ehleringer⁸, Tomas F. Domingues⁹, Jean Pierre H. B. Ometto⁴, Antonio D. Nobre⁴, Osvaldo Luiz Leal de Moraes¹⁰, Matthew Hayek¹¹, J. William Munger¹¹, Steve Wofsy¹¹

¹Department of Environmental Research and Innovation, Luxembourg Institute of Science and Technology (LIST), Belvaux, Luxembourg

²Department of Environmental, Social and Spatial Change, Roskilde University, Roskilde, Denmark

³Jet Propulsion Laboratory, California Institute of Technology, 4800 Oak Grove Drive, Pasadena, 91109, USA

⁴Instituto Nacional de Pesquisas Espaciais (INPE), Centro de Ciência do Sistema Terrestre, São José dos Campos, SP, Brazil

⁵Alterra, Wageningen University and Research Centre, Wageningen, The Netherlands

⁶Empresa Brasileira de Pesquisa Agropecuária (EMBRAPA), Belém-PA, Brazil

⁷Department of Ecology and Evolutionary Biology, University of Arizona, Tucson, AZ, USA

⁸Department of Biology, University of Utah, Salt Lake City, UT, USA

⁹Faculdade de Filosofia Ciências e Letras de Ribeirão Preto, Universidade de São Paulo (USP), São Paulo, SP, Brazil

¹⁰Centro Nacional de Monitoramento e Alertas de Desastres Naturais, SP-RJ, Brazil

¹¹Harvard University, Cambridge, MA, USA

Corresponding Authors: Kaniska Mallick (Phone: +352 275888425; Email: kaniska.mallick@gmail.com); Ivonne Trebs (Phone: +352 275888880; Email: ivonne.trebs@list.lu)

Running head:

Bio-physical controls on evapotranspiration

Abstract:

Canopy and aerodynamic conductances (g_C and g_A) are two of the key land surface biophysical variables that control the land surface response of land surface schemes in climate models. Their representation is crucial for predicting transpiration (λE_T) and evaporation (λE_E) flux components of the terrestrial latent heat flux (λE), which has important implications for global climate change and water resource management. By physical integration of radiometric surface temperature (T_R) into an integrated framework of the Penman-Monteith and Shuttleworth-Wallace model Here, we present a novel approach to directly quantify the controls of the canopy-scale conductances on λE_T and λE_E over multiple plant functions types (PFTs) in the Amazon Basin. Combining data from six LBA (Large-scale Biosphere-Atmosphere Experiment in Amazonia) eddy covariance tower sites and a T_R -driven physically-based modeling approach ~~a physically-based modeling approach~~, we identified the canopy-scale feedback-response mechanism between g_C , λE_T , and atmospheric vapor pressure deficit (D_A), without using any leaf-scale empirical parameterizations for the modelling ~~which was originally postulated to occur at the leaf scale~~. The T_R -based model shows minor biophysical control on λE_T during the wet (rainy) seasons where λE_T becomes predominantly radiation driven and net radiation (R_N) determines 75% to 80% of the variances of λE_T . ~~We show minor biophysical control on λE_T under wet conditions where net radiation (R_N) determines 75% to 80% of the variances of λE_T .~~ However, biophysical control on λE_T is amplified-dramatically increased during the dry seasons, and particularly the 2005 drought year ~~(2005) and dry conditions~~, explaining 50% to 65% of the variances of λE_T and indicates λE_T to be substantially soil moisture driven during rainfall deficit phase. Despite substantial differences in g_A between forests and pastures, very similar canopy-atmosphere ‘coupling’ was found in these two biomes due to soil moisture induced decrease in g_C in the pasture. This revealed the pragmatic aspect of the T_R -driven model behavior which exhibits a

high sensitivity of g_C to per unit change in wetness as opposed to g_A that is not sensitive to surface wetness variability. Our results reveal the occurrence of a significant hysteresis effect between λE_T and g_C during the dry season for the pasture sites, which is attributed to relatively low soil water availability as compared to the rainforests, likely due to differences in rooting depth between the two systems. Evaporation was significantly influenced by g_A for all the PFTs and across all wetness conditions. Our analytical framework accurately captures the responses of g_C and g_A to changes in radiation forcings, D_A , and surface radiometric temperature, and thus appears to be promising for the improvement of existing land-surface-atmosphere exchange parameterisations across a range of spatial scales.

Keywords: Canopy conductance, aerodynamic conductance, transpiration, evaporation, Penman-Monteith, Shuttleworth-Wallace, coupling, Amazon, LBA

1 Introduction

The Amazon rainforest is one of the world's most extensive natural ecosystems influencing the Earth's water, energy, and carbon cycles (Malhi et al., 2012), and also a major source of global terrestrial evapotranspiration (E) or latent heat flux (λE) (Costa et al., 2010; Harper et al., 2014). An intensification of the Amazon hydrological cycle was observed in the past two decades~~An intensification of the Amazon hydrological cycle was observed in the past two decades characterised by increased temperatures and more frequent droughts and floods~~ (Cox et al., 2000; Huntingford et al., 2008; Gloor et al., 2013). Recent Amazonian droughts have gained particular attention due to the sensitivity of the tropical forest λE to climate change (Hilker et al., 2014). If persistent precipitation extremes become more prevalent (Hilker et al., 2014); the Amazon rainforest may increasingly become a net source of carbon~~A very recent study suggests that, in case of persistent precipitation extremes (Hilker et al., 2014), the Amazon forest may become an increasing carbon source~~ as a result of both the suppression of net biome exchange by drought and carbon emissions from fires (Gatti et al., 2014). Moreover, changes in land cover due to conversion of tropical forest to pastures significantly alters the energy partitioning of the region by decreasing λE and increasing sensible heat fluxes (H) over pasture sites (e.g. Priante-Filho et al., 2004). This will ultimately lead to severe consequences for the water balance in the region, with modifications to increased (or decreased) river discharge already observedprevailing in some parts of the Basin (Davidson et al., 2012). Evaluating the λE response to changing climate and land use in the Amazon basin is critical to understand the stability of the tropics within the Earth system (Lawrence and Vandecar, 2015). The control of λE can be viewed as complex supply-demand interactions, where net radiation and soil moisture represents the supply and the atmospheric vapor pressure deficit represents the demand. This supply-demand interaction accelerates the biophysical feedbacks in λE and understanding these biophysical feedbacks is necessary to

690 assess the terrestrial biosphere response to water availability. Therefore, quantifying the
691 critical role of biophysical variables on λE will add substantial insight to assessments of the
692 resilience of the Amazon basin under global change.

693 The aerodynamic and canopy conductances (g_A and g_C , hereafter) (unit m s^{-1}) are the two
694 most important biophysical ~~(biological + physical)~~ variables regulating the evaporation (λE_E)
695 and transpiration (λE_T) flux components of λE (Monteith and Unsworth, 2008; Dolman et al.,
696 2014; Raupach, 1995; Colaizzi et al., 2012; Bonan et al., 2014). While g_A controls the bulk
697 aerodynamic transfer of energy and water through the near-surface boundary layer, g_C
698 represents the restriction on water vapour flow through the aggregated conductance from

699 stomata of the leaves, in case of a ~~vegetation~~ vegetated surface. In case of partial vegetation
700 cover g_C also includes soil surface conductance for evaporation. At small g_C/g_A ratio, the
701 vapor pressure deficit close to the canopy source/sink height (D_0) approximates the
702 atmospheric vapor pressure deficit (D_A) due to aerodynamic mixing and/or low transpiration.
703 These results in a strong canopy-atmosphere coupling and such conditions are prevalent
704 under soil moisture deficits. On the contrary, large g_C/g_A ratio influences the gradients of
705 vapor pressure deficit just above the canopy, such that D_0 tend towards zero and thus remains
706 different from D_A (Jarvis and McNaughton, 1986). This situation reflects a weak canopy-
707 atmosphere coupling and such situations prevail under predominantly wet conditions and/or
708 poor aerodynamic mixing due to wetness induced low aerodynamic roughness. ~~In case of~~
709 ~~partial vegetation cover g_C also includes evaporation from soil surface.~~ The Penman-Monteith

710 (PM) equation is a physically-based scheme for quantifying the biophysical controls on
711 canopy-scale λE_E and λE_T from terrestrial ecosystems, treating the vegetation canopy as a
712 ‘big-leaf’ (Monteith, 1965; 1981). Despite its development based on biophysical principles
713 controlling water vapour exchange, quantifying the g_A and g_C controls on λE through the PM
714 equation suffers from the continued longstanding uncertainty over the aggregated stomatal

and aerodynamic behaviour within the soil-plant-atmosphere-continuum (Matheny et al., 2014; Prihodko et al., 2008).

One of the major sources of uncertainties in modeling g_A is associated with the empirical (and uncertain) parameterizations of near-surface boundary layer dynamics, which is invariably confounded by space-time variability in atmospheric stability (van der Tol et al., 2009; Shuttleworth, 1989; [Gibson et al., 2011](#)). For example, Monin-Obukhov Similarity Theory (MOST) appears to be only be valid over uniform, extensive, and flat surfaces (Monteith and Unsworth, 2008; van der Tol et al., 2009; Holwerda et al., 2012), and its application to complex ‘real’ canopy systems is problematic due to chaotic interactions between turbulence, canopy roughness and topography (Raupach and Finnigan, 1995; Shuttleworth, 2007; Holwerda et al., 2012). Similarly, g_C varies in space and time due to variations in plant species, photosynthetic capacity, soil moisture variability and environmental drivers (Monteith and Unsworth, 2008; van der Tol et al., 2009). Despite the existence of several semi-mechanistic and empirical parameterisations for g_C (e.g. Ball et al., 1987; Leuning, 1995; Tuzet et al., 2003; Medlyn et al., 2011), the adaptive tendencies of plant canopies severely compromises the efficacy of such approaches (Matheny et al., 2014), limiting their applicability over most landscapes. Thus, debate over the most appropriate model of canopy conductance has endured for decades.

Previous studies in the Amazon Basin focussed on [developing an](#) observational understanding of [the](#) biogeochemical cycling of energy, water, carbon, trace gases, and aerosols in Amazonia (Andreae et al., 2002; Malhi et al., 2002; da Rocha et al., 2009), model-based understanding of surface ecophysiological behaviour and seasonality of λE (Baker et al., 2013; Christoffersen et al., 2014), modelling the [environmental](#) controls on λE (Hasler and Avissar, 2007; Costa et al., 2010), understanding [the](#) seasonality of photosynthesis and of λE (da Rocha et al., 2004; Restrepo-Coupe et al., 2013) and the impact of land use on

hydrometeorology (Roy and Avissar, 2002; von Randow et al., 2012). However, the
 combination of climatic and ecohydrological disturbances will significantly affect ~~the~~
 stomatal functioning, the partitioning of λE_E - λE_T and carbon-water-climate interactions of
~~the~~ tropical vegetation (Cox et al., 2000; Mercado et al., 2009). Hence, investigation of the
 effects of drought and land cover changes on conductances, λE_E , and λE_T are topics requiring
 urgent attention (Blyth et al., 2010) both because of the cursory way it is handled in current
 generation of parametric models (Matheny et al., 2014) and because of the centrality of g_A
 and g_C in controlling modelled flux behaviours (Villagarcía et al., 2010). The persistent risk
of deforestation is likely to alter the radiation interception, surface temperature, surface
moisture, associated meteorological conditions, and vegetation biophysical states of different
plant functional types (PFTs). Conversion from forest to pasture is expected to change the
 g_C/g_A ratio of these ecosystems and impact the evapotranspiration components. Given the
~~persistent risk of deforestation, the ecophysiological changes of different plant functional~~
~~types (PFTs) are expected to be reflected in g_A and g_C and λE_E and λE_T .~~ Besides inverting the
 PM equation using field measurements of λE , till date either photosynthesis-dependent
modeling or up-to-date-only leaf-scale experiments were performed to directly quantify g_C
 (Ball et al., 1987; Meinzer et al., 1993, 1997; Monteith, 1995; Jones, 1998; Motzer et al.,
 2005). However, an analytical or physical retrieval for g_A and g_C is required not only to better
understand the role of the canopy in regulating evaporation and transpiration, but to enable a
capability to characterize the conductances using remote observations, across large spatial
domains where in-situ observations are not available.~~However, an analytical or physical~~
~~retrieval for g_A and g_C required to understand the role of the canopy in regulating evaporation~~
~~and transpiration of water is still lacking.~~ This paper aims to leverage this emerging
 opportunity by exploring data from the Large-scale Biosphere-Atmosphere Experiment in
 Amazonia (LBA) eddy covariance (EC) observations (e.g., de Gonçalves et al., 2013;

Restrepo-Coupe et al., 2013) using a novel analytical modeling technique, the Surface Temperature Initiated Closure (STIC) (STIC1.0 and STIC1.1) (Mallick et al., 2014, 2015) in order to quantify the biophysical control on λE_E and λE_T over several representative PFTs of the Amazon Basin.

STIC provides a framework for simultaneously retrieving g_A and g_C , and surface energy balance fluxes. It is based on finding analytical solutions for g_A and g_C by physically integrating radiometric surface temperature (T_R) information (along with radiative fluxes, meteorological variables) into the PM model (Mallick et al., 2014, 2015). The direct estimates of canopy-scale conductances and λE obtained through STIC are independent of any land surface parameterisation. *This contrasts with the multi-layer canopy models that explicitly parameterize the leaf-scale conductances and perform bottom-up scaling to derive the canopy-scale conductances (Baldocchi et al., 2002; Drewry et al., 2010).* A primary advantage of the approach on which STIC is based is the ability to directly utilize remotely sensed T_R to estimate E , thereby providing a capability to estimate E over large spatial scales using a remotely sensed variable that is central to many ongoing and upcoming missions. This study presents a detailed examination of the performance of STIC to better understand land-atmosphere interactions in one of the most critical global ecosystems and addresses the following science questions and objectives:

~~This study addresses the following science questions and objectives:~~

(1) How realistic are ~~the~~ canopy-scale conductances ~~and their behaviour~~ when estimated analytically (or non-parametrically) without involving any empirical leaf-scale parameterization?

(2) What are the controls of canopy-scale g_A and g_C on evaporation and transpiration in the Amazon basin, as evaluated using STIC?

(3) How do the STIC-based canopy-scale conductances compare with known ~~(or believed)~~ environmental constraints?

(4) Is the ~~biological~~ biophysical response of g_C consistent with the leaf-scale theory (Jarvis and McNaughton, 1986; McNaughton and Jarvis, 1991; Monteith, 1995)?

The following section describes a brief methodology to retrieve g_C , g_A , λE_E , and λE_T . The data sources used for the analysis are described after the methodology and will be followed by a comparison of the results with fluxes derived from EC measurements. A detailed discussion of the results and potential applicability of the method with implications for global change research are elaborated at the end. A list of symbols and variables used in the present study is given in Table 1.

2 Methodology

2.1 Theory

The retrieval of g_A , g_C , and λE are based on finding a ‘closure’ of the PM equation (eq. 1 below) using the STIC framework (Fig. A1 in Appendix Fig. A1) (Mallick et al., 2015). STIC is a physically-based single-source surface energy balance scheme which includes internally consistent estimation of g_A and g_C (Mallick et al., 2014, 2015). Originally designed for application to thermal remote sensing data from Earth observation sensors, the STIC framework exploits observations of radiative (T_R), ~~T_{R^*} -radiative~~, and environmental variables including net radiation (R_N), ground heat flux (G), air temperature (T_A), relative humidity (R_H) or vapor pressure (e_A) at a reference level above the surface.

The foundation of the development of STIC is based on the goal of finding an analytical solution of the two unobserved ‘state variables’ (g_A and g_C) in the PM equation while exploiting the radiative (R_N and G), meteorological (T_A , R_H), and radiometric surface temperature (T_R) as external inputs. The fundamental assumption in STIC is the first order

dependence of g_A and g_C on the aerodynamic temperature (T_0) and soil moisture (through T_R). This assumption allows a direct integration of T_R into the PM equation while simultaneously constraining the conductances through T_R . Although the T_R signal is implicit in R_N , which appears in the numerator of the PM equation (eqn. 1), it may be noted that R_N has a relatively weak dependence on T_R (compared to T_R sensitivities of soil moisture and λE). Given T_R is the direct signature of the soil moisture availability, inclusion of T_R in the PM equation also works to add water stress controls in g_C . Until now the explicit use of T_R in the PM model was hindered due to the unavailability of any direct method to integrate T_R into this model, and, furthermore, due to the lack of physical models expressing biophysical states of vegetation as a function of T_R . Therefore, the majority of the PM-based λE modeling approaches strongly rely on surface reflectance and meteorology while exploiting the empirical leaf-scale parameterisations of the biophysical conductances (Prihodko et al., 2008; Bonan et al., 2014; Ershadi et al., 2015).

The PM equation is commonly expressed as,

$$\lambda E = \frac{s\phi + \rho c_p g_A D_A}{s + \gamma \left(1 + \frac{g_A}{g_C}\right)} \quad (1)$$

where ρ is the air density (kg m^{-3}), c_p is the specific heat of air ($\text{J kg}^{-1} \text{K}^{-1}$), γ is the psychrometric constant (hPa K^{-1}), s is the slope of the saturation vapor pressure versus air temperature (hPa K^{-1}), D_A is the saturation deficit of the air (hPa) or vapor pressure deficit at the reference level, and ϕ is the net available energy (W m^{-2}) (the difference between R_N and G). The units of all the surface fluxes and conductances are in W m^{-2} and m s^{-1} , respectively.

For a dense canopy, g_C in the PM equation represents the canopy surface conductance. Although it is not equal to the canopy stomatal conductance, it contains integrated information of the stomata. For a heterogeneous landscape, g_C in the PM equation is an aggregated surface conductance containing information on both canopy and soil.

Traditionally, the two unknown ‘state variables’ in eqn. (1) are g_A and g_C , and the STIC methodology is based on formulating ‘state equations’ for these conductances that satisfy the PM model (Mallick et al., 2014, 2015).

The PM equation is ‘closed’ upon the availability of canopy-scale measurements of the two unobserved biophysical conductances, and if we assume the empirical models of g_A and g_C to be reliable. However, neither g_A nor g_C can be measured at the canopy-scale or at larger spatial scales. Furthermore, as shown by some recent studies (Matheny et al., 2014; van Dijk et al., 2015), a more appropriate g_A and g_C model is currently not available. This implies that a true ‘closure’ of the PM equation is only possible through an analytical estimation of the conductances. Traditionally, the two unknowns in eq. 1 are g_A and g_C . Therefore, the STIC methodology is based on formulating state equations (eq. 2 to 5 below) for these conductances that satisfy the PM equation (for detailed derivations of eq. 2 to 5 see Mallick et al., 2014, 2015).

2.2 State equations

By integrating T_R with standard surface energy balance (SEB) theory and vegetation biophysical principles, STIC formulates multiple ‘state equations’ that eliminate the need for exogenous parametric submodels for g_A and g_C , associated aerodynamic variables, and land-atmosphere coupling. The state equations of STIC are as follows and their detailed derivations are described Appendix (A1).

$$g_A = \frac{\phi}{\rho c_p \left[(T_o - T_A) + \left(\frac{e_o - e_A}{\gamma} \right) \right]} \quad (2)$$

$$g_C = g_A \frac{(e_o - e_A)}{(e_o^* - e_o)} \quad (3)$$

$$T_o = T_A + \left(\frac{e_o - e_A}{\gamma} \right) \left(\frac{1 - \Lambda}{\Lambda} \right) \quad (4)$$

$$\Lambda = \frac{2\alpha s}{2s + 2\gamma + \gamma \frac{g_A}{g_C} (1 + M)} \quad (5)$$

Here, T_0 is the temperature ($^{\circ}\text{C}$) at the source/sink height (or at the roughness length (z_0) or in-canopy air stream), e_0 is the atmospheric vapor pressure (hPa) at the source/sink height, e_0^* is the saturation vapor pressure (hPa) at the source/sink height, Λ is the evaporative fraction (the ratio of λE and ϕ), α is the Priestley-Taylor parameter (unitless) (Priestley and Taylor, 1972), and M is a unitless quantity which describes the relative wetness (or moisture availability) of the surface. M controls the transition from potential to actual evaporation and hence is critical for providing the constraint against which the conductances can be estimated (M estimation is explained in Appendix A2).

Given the values of R_N , G , T_A , and R_H or e_A , the four state equations (eqn. 2 to 5) can be solved simultaneously to derive analytical solutions for the four state variables. This also produces a ‘closure’ of the PM model, which is independent of empirical parameterizations for both g_A and g_C . However, the analytical solution to the above state equations have four accompanying unknowns; M (surface moisture availability), e_0 (vapor pressure at the source/sink height), e_0^* (saturation vapor pressure at the source/sink height), and Priestley-Taylor coefficient (α), and as a result there are 4 equations with 8 unknowns. Consequently an iterative solution is needed to determine the four unknown variables (as described in Appendix A2), which is a further modification of the STIC1.1 framework (Mallick et al., 2015). The present version of STIC is designated as STIC1.2 and its uniqueness is the physical integration of T_R into a combined structure of the PM and Shuttleworth-Wallace (SW, hereafter) (Shuttleworth and Wallace, 1985) model to estimate the source/sink height vapor pressures (Appendix A2). In addition to physically integrating T_R observations into a combined PM-SW framework, STIC1.2 also establishes a feedback loop describing the relationship between T_R and λE , coupled with canopy-atmosphere components relating λE to

T_0 and e_0 . For estimating M , the radiometric surface temperature (T_R) is extensively used in a physical retrieval framework, thus treating T_R as an external input. In eqn. (5), the Priestley-Taylor coefficient (α) appeared due to the use of the Advection-Aridity (AA) hypothesis (Brutsaert and Stricker, 1979) for deriving the state equation of Λ (Supplement S1). However, instead of optimising α as a ‘fixed parameter’, we have developed a physical equation of α (eqn. A15 in the Appendix A2) and numerically estimated α as a ‘variable’. The derivation of the equation for α is described in Appendix A2. The fundamental differences between STIC1.2 and earlier versions are described in Table (A1).

In STIC1.2, T_0 is a function of T_R and they are not assumed equal ($T_0 \neq T_R$). The analytical expression of T_0 is dependent on M and the estimation of M is based on T_R . To further elaborate this point on the inequality of T_0 and T_R , we show an intercomparison of retrieved T_0 versus T_R for forest and pasture (Fig. A2). This indicates the distinct difference of the retrieved T_0 from T_R for the two different biomes. ~~Given the information of R_N , G , T_A , R_H or e_A , and T_R , these state equations can be solved simultaneously to derive analytical solutions for g_A and g_C . This also produces a ‘closure’ of the PM model, which is independent of empirical parameterizations for both g_A and g_C . The analytical solution to the state equations 2-5 have three additional unknowns; e_0^* , e_0 , and α , and these variables are iteratively estimated as described in the Appendix, which is also a modification of the STIC1.1 framework (Mallick et al., 2015). The present version of STIC is designated as STIC1.2. STIC uses T_R as an additional data source to retrieve M and the estimation of M is also explained in the Appendix. The detailed derivations of the state equations (eq. 2 to 5) of STIC are described in Mallick et al. (2014; 2015).~~

2.2.3 Partitioning λE

The terrestrial latent heat flux is an aggregate of both transpiration (λE_T) and evaporation (λE_E) (sum of soil evaporation and interception evaporation from canopy). During rain events the land surface becomes wet and λE tends to approach the potential evaporation (λE^*), while surface drying after rainfall causes λE to approach the potential transpiration rate (λE_T^*) in the presence of vegetation, or zero without any vegetation. Hence, λE at any time is a mixture of these two end member conditions depending on the degree of surface moisture availability or wetness (M) (Bosveld and Bouten, 2003; Loescher et al., 2005). Considering the general case of evaporation from any ~~nonsaturated~~ unsaturated surface at a rate less than the potential, M is the ratio of the actual to the potential evaporation rate and is considered as an index of evaporation efficiency during a given time interval (Boulet et al., 2015). Partitioning of λE into λE_E and λE_T was performed according to Mallick et al. (2014) as follows:

$$\lambda E = \lambda E_E + \lambda E_T = M \lambda E^* + (1 - M) \lambda E_T^* \quad (6)$$

The estimates of λE_E in the current method consists of aggregated contribution from both interception and soil evaporation, and no further attempt is made to separate these two components. In the Amazon forest, ‘soil evaporation’ has a negligible contribution while the ‘interception evaporation’ contributes substantially to the total evaporative fluxes, and, therefore the partitioning of λE into λE_E and λE_T is crucial. After estimating g_A , λE^* was estimated according to the Penman equation and λE_T was estimated as the residual in equation 6.

In this study, we use the term ‘canopy conductance’ instead of ‘stomatal conductance’ given the term ‘stomata’ is applicable at the leaf-scale only. It is important to appreciate that g_C should principally be a mixture of the stomatal (or biological) and soil conductances. However, given the high vegetation density of the Amazon Basin, the soil surface exposure is

negligible, and, hence we assume g_C to be the canopy-scale aggregate of stomatal conductance. Similarly, different g_A exists for soil-canopy, sun-shade, and dry-wet conditions (Leuning, 1995); which is currently integrated into a lumped g_A (given the big-leaf nature of STIC). From the big-leaf perspective, it is generally assumed that the aerodynamic conductance of water vapor and heat are equal (Raupach, 1998). However, for obtaining partitioned aerodynamic conductances, explicit partitioning of λE is needed, which is beyond the scope of the current manuscript.

2.4.3 Evaluating g_A and g_C

Due to the lack of direct canopy-scale g_A measurements, a rigorous evaluation of g_A cannot be performed. To evaluate the STIC retrievals of g_A (g_{A-STIC}) we adopted three different methods:

(a) By ~~exploring~~ using the measured friction velocity (u^*) and wind speed (u) at the EC towers and using the equation of Baldocchi and Ma (2013) (g_{A-BM13}) in which g_A was expressed as sum of turbulent conductance and canopy (quasi-laminar) boundary layer conductance as,

$$g_{A-BM13} = [(u/u^{*2}) + (2/ku^{*2})(S_c/P_r)^{0.67}]^{-1} \quad (7)$$

where k is von Karman's constant, 0.4; S_c is the Schmidt Number; P_r is the Prandtl Number and their ratio is generally considered to be unity. Here the conductances of momentum, sensible and latent heat fluxes are assumed to be identical (Raupach, 1998).

(b) By inverting λE observations for wet conditions hence assuming $\lambda E \cong \lambda E^*$ and estimating g_A (g_{A-INV}) as,

$$g_{A-INV} = \gamma \lambda E / \rho c_p D_A \quad (8)$$

(c) By inverting the aerodynamic equation of H and estimating a hybrid g_A (g_{A-HYB}) from observed H and STIC T_0 as (T_{0-STIC}),

$$g_{A-HYB} = H/\rho c_p (T_{0-STIC} - T_A) \quad (9)$$

Like g_{A-STIC} , direct verification of STIC g_C (g_{C-STIC}) could not be performed as canopy-scale g_C observations are not possible with current measurement techniques. Although leaf-scale g_C measurements are relatively straightforward, these values are not comparable to values retrieved at the canopy-scale. However, assuming u^* -based g_A as baseline aerodynamic conductance, we have estimated canopy-scale g_C by inverting the PM equation (g_{C-INV}) (Monteith, 1995) to evaluate g_{C-STIC} by exploiting g_{A-BMI3} in conjunction with the available ϕ , λE , T_A , and D_A measurements from the EC towers. Similarly, we compared the STIC-derived g_C (g_{C-STIC}) with g_C estimated by inverting the PM model (g_{C-INV}) (Monteith, 1995) exploiting g_{A-BMI3} in conjunction with the available ϕ , λE , T_A , and D_A measurements from the EC towers.

2.5 Decoupling coefficient and biophysical controls

The decoupling coefficient or ‘Omega’ (Ω) is a dimensionless coefficient ranging from 0.0 to 1.0 (Jarvis and McNaughton, 1986) and considered as an index of the degree of stomatal control on transpiration relative to the environment. The equation of Ω is as follows:

$$\Omega = \frac{\frac{s}{\gamma} + 1}{\frac{s}{\gamma} + 1 + \frac{g_A}{g_C}} \quad (10)$$

Introducing Ω in the Penman-Monteith (PM) equation for λE results in:

$$\lambda E = \Omega \lambda E_{eq} + (1 - \Omega) \lambda E_{imp} \quad (11)$$

$$\lambda E_{eq} = \frac{s\phi}{s + \gamma} \quad (12)$$

$$\lambda E_{imp} = \frac{\rho c_p}{\gamma} g_C D_A \quad (13)$$

Where, λE_{eq} is the equilibrium latent heat flux, which depends only on ϕ and would be obtained over an extensive surface of uniform moisture availability (Jarvis and McNaughton,

1986; Kumagai et al., 2004). λE_{imp} is the imposed latent heat flux, which is ‘imposed’ by the atmosphere on the vegetation surface through the effects of vapor pressure deficit (triggered under limited soil moisture availability) and λE becomes proportional to g_C .

When the g_C/g_A ratio is very small (i.e., water stress conditions), stomata principally control the water loss and a change in g_C will result in a nearly proportional change in transpiration. Such conditions trigger strong biophysical control on transpiration. In this case the Ω value approaches zero and vegetation is believed to be fully coupled to the atmosphere. In contrast, for a high g_C/g_A ratio (i.e., high water availability), changes in g_C will have little effects on the transpiration rate, and transpiration is predominantly controlled by ϕ . In this case the Ω value approaches unity, and vegetation is considered to be poorly coupled to the atmosphere.

Given both g_A and g_C are the independent estimates in STIC1.2, the concept of Ω was used to understand the degree of biophysical control on λE_T , which indicates the extent to which the transpiration fluxes are approaching the equilibrium limit. However, the biophysical characterisation of λE_T and λE_E through STIC1.2 significantly differs from previous approaches (Ma et al., 2015; Chen et al., 2011; Kumagai et al., 2004), and the fundamental differences are centered on the specifications of g_A and g_C (as described in Table A2). While the estimation of g_A in previous approaches is based on u and u^* , the estimation of g_C was based on inversion of observed λE based on the PM equation (e.g. Stella et al., 2013). However, none of these approaches allow independent quantification of biophysical controls of λE as g_C is constrained by λE itself.

3 Datasets

3.1 Eddy covariance and meteorological quantities

We ~~have~~ used the LBA (Large-Scale Biosphere-Atmosphere Experiment in Amazonia) data for quantifying the biophysical controls on the evaporative flux components. LBA ~~is~~ was an

international research initiative conducted from 1995-2005 to study how Amazonia functions as a regional entity within the larger Earth system, and how changes in land use and climate will affect the hydrological and biogeochemical functioning of the Amazon ecosystem (Andreae et al., 2002).

A network of eddy covariance (EC) towers was operational during the LBA experiment, such that data from nine EC towers were obtained from the ORNL Distributed Archive Active Centre (ftp://daac.ornl.gov/data/lba/carbon_dynamics/CD32_Brazil_Flux_Network/). These are the quality controlled and harmonized surface flux and meteorological data from the Brazilian Amazon flux network. Time series of surface fluxes (λE , H , G), radiation (T_R , R_N , shortwave and longwave), meteorological quantities (T_A , R_H , wind speed) as well as soil moisture and rainfall were available from six (out of nine) EC towers. Three of the EC towers had numerous missing data and were not included in the analysis. The surface energy balance was closed by applying the Bowen ratio (Bowen, 1926) closure as described in Chavez et al. (2005) and later adopted by Anderson et al. (2007) and Mallick et al. (2015). In the absence of G measurements, ϕ was assumed to be equal to the sum of λE and H with the assumption that a dense vegetation canopy restricts the energy incident on the soil surface, thereby allowing us to assume negligible ground heat flux. For the present analysis, data from six selected EC towers (Table 2) represent two different biomes (forest and pasture) covering four different PFTs, namely, tropical rainforest (TRF), tropical moist forest (TMF), tropical dry forest (TDF), and pasture (PAS), respectively. A general description of the datasets can be found in Saleska et al. (2013). For all sites, monthly averages of the diurnal cycle (hourly time resolution) were chosen for the present analysis.

4 Results

4.1 Evaluating g_A , g_C and surface energy balance fluxes

Examples of monthly averages of the diurnal cycles of the four different g_A estimates and their corresponding g_C estimates over two different PFTs (K34 for forest and FNS for pasture) reveal that g_{A-STIC} and g_{C-STIC} tend to be generally higher over the forest than their counterparts, varying from 0 to 0.06 m s⁻¹ and 0 to 0.04 m s⁻¹ respectively (Fig. 1a and 1b). The magnitude of g_{A-STIC} varied between 0 to 0.025 m s⁻¹ for the pasture (Fig. 1a), while g_{C-STIC} values were less than half that of those estimated over the forest (0 – 0.01 m s⁻¹) (Fig. 1b). The conductances showed a marked diurnal variation expressing their overall dependence on net radiation, vapor pressure deficit, and surface temperature. Despite the absolute differences between the conductances from the different retrieval methods, their diurnal patterns were comparable.

The canopy-scale evaluation of g_{A-STIC} is illustrated in Fig. 2a (and Table 3) combining data from the four PFTs. Estimated values range between zero and 0.1 m s⁻¹ and show modest correlation ($R^2 = 0.44$) (R^2 range between 0.22 [± 0.18] to 0.55 [± 0.12]) between g_{A-BMI3} and g_{A-STIC} with regression parameters ranging between 0.81 (± 0.023) and 1.07 (± 0.047) for the slope and 0.0019 (± 0.0006) to 0.0006 (± 0.0006) m s⁻¹ for the offset (Table 3). The root mean squared deviation (RMSD) varied between 0.007 (TDF) and 0.013 m s⁻¹ (TRF). Statistical comparisons between g_{A-STIC} and g_{A-HYB} revealed relatively low RMSD and high correlation between them (RMSD = 0.007 m s⁻¹ and $R^2 = 0.77$) as compared to the error statistics between g_{A-STIC} and g_{A-INV} (RMSD = 0.011 m s⁻¹ and $R^2 = 0.50$) (Fig. 2b, 2c). The residuals between g_{A-STIC} and g_{A-BMI3} are plotted as a function of u and u^* in Fig. (2d) with the aim to ascertain whether significant biases are introduced by ignoring wind and shear information within STIC1.2. As illustrated in Fig. 2d, there appears to be a weak systematic relationship between the residual g_A difference with either u^* or u ($r = -0.26$ and -0.17). However, a

considerable relationship was found between wind and shear driven g_A (i.e., g_{A-BM13}) versus ϕ , T_R and D_A ($r = 0.83, 0.48$, and 0.42) (Fig. 2e and 2f), which indicates that these three energy and water constraints can explain 69%, 23%, and 17% variance of g_{A-BM13} .

Canopy-scale evaluation of hourly g_C is presented in Fig. 3a (and Table 3) combining data from the four PFTs. Estimated values range between zero and 0.06 m s^{-1} for g_{C-STIC} and show reasonable correlation ($R^2 = 0.39$) (R^2 range between $0.14 [\pm 0.04]$ to $0.58 [\pm 0.12]$) between g_{C-STIC} and g_{C-INV} with regression parameters ranging between $0.30 (\pm 0.022)$ and $0.85 (\pm 0.025)$ for the slope and $0.0024 (\pm 0.0003)$ to $0.0097 (\pm 0.0007) \text{ m s}^{-1}$ for the offset (Table 3). The RMSD varied between 0.007 (PAS) and 0.012 m s^{-1} (TRF and TDF). Given g_A significantly controls g_C , we also examined whether biases in g_C are introduced by ignoring wind and shear information within STIC. The scatterplots between residual g_C difference ($g_{C-STIC} - g_{C-INV}$) versus both u and u^* (Fig. 3b) showed g_C residuals to be evenly distributed across the entire range of u and u^* and no systematic pattern was evident.

The reliability of ~~the~~ STIC1.2--based g_A and g_C retrievals was further verified by evaluating λE and H estimates (Fig. 4). Both the predicted λE and H are generally in good agreement with the observations, with substantial correlation (r) (R^2 from 0.61 to 0.94), ~~acceptable~~ reasonable RMSD of 33 and 37 W m^{-2} , and mean absolute percent deviation (MAPD) of 14% and 32% between the observed and STIC fluxes (Fig. 4). Regression parameters varied between $0.96 (\pm 0.008)$ to $1.14 (\pm 0.010)$ for the slope and $-16 (\pm 2)$ to $-2 (\pm 2) \text{ W m}^{-2}$ for the offset for λE (Table 4), whereas for H , these were $0.60 (\pm 0.025)$ to $0.89 (\pm 0.035)$ for the slope and $9 (\pm 1)$ to $29 (\pm 2) \text{ W m}^{-2}$ for the offset (Table 3), respectively. The RMSD in λE varied from 20 to 31 W m^{-2} and 23 to 34 W m^{-2} for H (Table 3).

The evaluation of the conductances and surface energy fluxes indicates some efficacy for the STIC derived fluxes and conductance estimates which represent a weighted average of these

variables over the source area around EC tower. ~~As a result we feel some justification for exploring the canopy scale biophysical controls on λE_T and λE_E generated through the STIC1.2 framework.~~

4.2 Canopy coupling, transpiration and evaporation

From Fig. 5a an overall weak to moderate relationship ($r = -0.31$ to -0.42) is apparent between the coupling (i.e., $1-\Omega$) and λE_T , where λE_T is negatively related to the coupling for all the PFTs, thus indicating the influence of weak to moderate biophysical controls on λE_T throughout the year in addition to ~~the~~ radiative controls. The biophysical control was substantially enhanced in TRF (r increased from -0.36 to -0.53 and -0.60) (47 to 67% increase) and TMF (r increased from -0.31 to -0.53 and -0.58) (70 to 85% increase) during the dry seasons (July-September) (Fig. 5a). A profound increase of biophysical control on λE_T during the dry season was also found in TDF (52% increase) and PAS (37% increase) (Fig. 5a). The negative relationship ($r = -0.29$ to -0.45) between $(1-\Omega)$ and λE_E (Fig. 5b) in all four PFTs indicated the role of aerodynamic control on λE_E . The aerodynamic control was also enhanced during the dry seasons as shown by the increased negative correlation ($r = -0.50$ to -0.69) (Fig. 5b) between $(1-\Omega)$ and λE_E .

Illustrative examples of the diurnal variations of λE_E , λE_T , and Ω for two different PFTs with different annual rainfall (2329 mm in rainforest, K34 and 1597 mm in pasture, FNS) for three consecutive days during both dry and wet seasons are shown in Fig. 5c to 5f. This shows morning rise of Ω and a near-constant afternoon Ω in the wet season (Fig. 5c and 5d), thus indicating no biophysical controls on λE_E and λE_T during this season. On the contrary, during the dry season, the morning rise in Ω is followed by a decrease during noontime (15% to 25% increase in coupling in forest and pasture) (Fig. 5e and 5f) due to dominant biophysical control, which is further accompanied by a transient increase from mid-afternoon till late

afternoon and steadily declined thereafter. Interestingly, coupling was relative higher in pasture during the dry seasons the reasons of which is detailed in the following section and discussion.

4.3 g_C and g_A versus transpiration and evaporation

Scatter plots between λE_T and λE_E versus g_C and g_A showed a triangular pattern which became wider with increasing ~~the~~ conductances (Fig. 6). To explain this ~~typical~~ behaviour of λE_T versus g_C and g_A , we further examined the entire mechanism of conductance- λE_T interactions through two dimensional scatters between λE_T and conductances for two consecutive diurnal cycles during wet and dry seasons over rainforest and pasture sites with different annual rainfall (e.g., K34 as wet and FNS as dry site, annual rainfall 2329 mm and 1597 mm) (Fig. 7). Our results confirm the occurrence of diurnal hysteresis between g_C - g_A and λE_T and explain the reason for the shape of the curves obtained in Fig. 6. During the wet season, a distinct environmental control is detectable on g_C and λE_T in the morning hours (Fig. 7a and 7b) in both PFTs where g_C and λE_T increased as a result of increasing R_N , T_R , and D_A . From the late morning to afternoon, a near-constant (forest) or negligible increase (pasture) of λE_T is observed despite substantial reduction of both g_C and g_A (25 to 50% decrease), after which λE_T starts decreasing. This behaviour of λE_T was triggered due to the concurrent changes in R_N (15 to 50% change), D_A (20 to 60% change) and surface temperature (T_R) (5% to 14% change), which indicates the absence of any dominant biophysical regulation on λE_T during the wet season (Fig. 7a and 7b). On the contrary in the dry season, although the morning rise in λE_T is steadily controlled by the integrated influence of environmental variables, but a modest to strong biophysical control is found for both PFTs during the afternoon where λE_T substantially decreased with decreasing conductances (Fig. 7c and 7d). This decrease in λE_T is mainly caused by the reduction in g_C as a result of

increasing D_A and T_R (as seen later in Fig. 8a and 8c). In the dry season, the area under the hysteretic relationship between λE_T , g_C and environmental variables was substantially wider in pasture (Fig. 7d) than for the rainforest (Fig. 7c), which is attributed to greater hysteresis area between R_N and D_A in pasture as a result of reduced water supply. The stronger hysteresis effects in pasture during the dry season (Fig. 7d) ultimately led to the stronger relationship between coupling and λE_T (as seen in Fig. 5a).

4.4 Factors affecting variability of g_C and g_A

The sensitivity of stomatal conductance to vapor pressure deficit is a key governing factor of transpiration (Ocheltree et al., 2014; Monteith, 1995). We examined if the feedback or feed-forward response hypothesis (Monteith, 1995; Farquhar, 1987) between g_C , D_A , and λE_T is reflected in our canopy-scale g_C retrievals. Combining data of all PFTs, we found an exponential decline of g_C in response to increasing D_A regardless of the variations of net radiation (Fig. 8a). High g_C is consistent with high humidity and low evaporative demand. Five negatively logarithmic scatters fit the data with r values of 0.38 ($0 < R_N < 150 \text{ W m}^{-2}$), 0.63 ($150 < R_N < 300 \text{ W m}^{-2}$), 0.73 ($300 < R_N < 450 \text{ W m}^{-2}$), 0.78 ($450 < R_N < 600 \text{ W m}^{-2}$), and 0.87 ($R_N > 600 \text{ W m}^{-2}$). The sensitivity of g_C to D_A was at the maximum in the high R_N range beyond 600 W m^{-2} and the sensitivity progressively declined with declining magnitude of R_N ($0 - 150 \text{ W m}^{-2}$).

Scatter plots between g_C and λE_T for different levels of D_A revealed a linear pattern between them for a wide range of D_A ($20 > D_A > 0 \text{ hPa}$) (Fig. 8b). Following Monteith (1995), isopleths of R_N are delineated by the solid lines passing through λE_T on the x-axis and through g_C on the y-axis. Isobars of D_A (dotted lines) pass through the origin because λE_T approaches zero as g_C approaches zero. Figure (8b) shows substantial reduction of g_C with increasing D_A without any increase of λE_T , like an inverse hyperbolic pattern to D_A (Monteith 1995; Jones,

1998). For all the PFTs, an active biological (i.e., stomatal) regulation maintained almost constant λE_T when D_A was changed from low to high values (Fig. 8b). At high D_A (above 10 hPa), after an initial increase of λE_T with g_C , g_C approached a maximum limit and remained nearly independent of λE_T (Fig. 8b). Among all the D_A levels, the maximum control of g_C on λE_T variability (62 to 80%) was found at high atmospheric water demand (i.e., 30 hPa > D_A > 20 hPa). The scatter plots between g_C and ~~radiometric surface temperature~~ (T_R) (Fig. 8c) for different levels of D_A revealed an exponential decline in g_C with increasing T_R and atmospheric water demand. When retrieved g_A was plotted against the radiometric surface temperature and air temperature difference ($T_R - T_A$), an exponential decline in g_A was found in response to increasing ($T_R - T_A$) (Fig. 8d). High g_A is persistent with low ($T_R - T_A$) irrespective of the variations in R_N (with the exception of very low R_N). Four negatively logarithmic scatters fit g_A versus ($T_R - T_A$) relationship with r values of 0.28 ($150 < R_N < 300$ W m⁻²), 0.55 ($3000 < R_N < 450$ W m⁻²), 0.64 ($450 < R_N < 600$ W m⁻²), and 0.77 ($R_N > 600$ W m⁻²).

5 Discussion

5.1 Evaluating g_A , g_C , and surface energy balance fluxes

In this paper, we have estimated the canopy-scale biophysical conductances and quantified their controls on the terrestrial evaporation components in a simplified surface energy balance modeling perspective that treats the canopy as ‘big leaf’. The aerodynamic conductance retrieved with STIC showed acceptable correlation and valid estimates of g_A when compared against an empirical model that uses u^* and u to derive g_A (Fig. 1 and 2a) and two other inversion/hybrid-based g_A estimates. The differences between g_{A-STIC} and g_{A-BM13} were mainly attributed to the structural differences and empirical nature of the parameterization for the near-surface boundary layer conductance ($((2/ku^*)^2)(S_c/P_r)^{0.67}$) in g_{A-BM13} , which results in some discrepancies between g_{A-STIC} and g_{A-BM13} particularly in the pasture (Fig. 2a). The extent to

which the structural discrepancies between g_{A-STIC} and g_{A-BM13} relate to actual differences in the conductances for momentum vs. heat is beyond the scope of this manuscript, and a detailed investigation using data on atmospheric profiles of wind speed, temperature etc. are needed to actually quantify such differences. Momentum transfer is associated with pressure forces and not identical to heat and mass transfer (Massman, 1999). In STIC1.2, g_A is directly estimated and is a robust representative of the conductances to heat/water vapor transfer; whereas g_{A-BM13} estimates based on u^* and u is more representative for the momentum transfer. Therefore, the difference between the two different g_A estimates (Fig. 2) can be largely attributed to the actual difference in the conductances for momentum and heat/water vapor. The turbulent conductance equation (u^{*2}/u) in g_{A-BM13} is also very sensitive to the uncertainties in the sonic anemometer measurement (Contini et al., 2006; Richiardone et al., 2012). However, the evidence of a weak systematic relationship between the g_A residuals and u (Fig. 2d) and thermal (T_R), radiative (ϕ), and meteorological (T_A , D_A) variables in capturing the variability of g_{A-BM13} (Fig. 2e and 2f) indicates the diagnostic potential g_{A-STIC} estimates to explain the wind driven g_A variability. ~~capability of the environmental variables (particularly ϕ , T_R , and D_A) in capturing the variability of g_{A-BM13} (Fig. 2e and 2f) indicates that g_{A-STIC} estimates are reliable despite neglecting u .~~ Excluding u might introduce errors in cases where wind is the only source of variations in g_A and surface fluxes (Mallick et al., 2015). In general, the accuracies in commonly used parametric g_A estimates based on u and surface roughness parameters several meters distant from canopy foliage is limited due to the uncertainties concerning the attenuation of u close to the vegetation surface (Meinzer et al., 1997; Prihodko et al., 2008). The magnitude of u near the foliage can be substantially lower than that measured considerably away at some reference location above or within the canopy (Meinzer et al., 1997). Notwithstanding the inequalities of g_A estimated with different methods, it is challenging to infer the accuracy of the different estimates. It is imperative to

mention that g_A is one of the main anchors in the PM-SW model because it not only appears in the numerator and denominator of these models, g_A also provides feedback to g_C , T_0 , and D_0 (seminal paper of Jarvis and McNaughton, 1986). Therefore, the estimates of λE in the PM-SW framework are very sensitive to parameterization of g_A and stable λE estimates might be possible if g_A estimation is unambiguous (Holwerda et al., 2012; van Dijk et al., 2015). Given the lack of consensus in the community on the ‘true’ g_A and from the nature of surface flux validation results (Fig. 4) it appears that g_{A-STIC} tends to be the appropriate aerodynamic conductance that satisfies the PM-SW equation. ~~However, from the surface flux validation results (Fig. 4) it appears that g_{A-STIC} is the appropriate aerodynamic conductance satisfying the PM equation.~~ Discrepancies between g_{C-STIC} and g_{C-INV} originated from the differences in g_A estimates between the two methods.

Despite the good agreement between the measured and predicted λE and H (Fig. 4, Table 3), the larger error in H was associated with the higher sensitivity of H to the errors in T_R (due to poor emissivity correction) (Mallick et al., 2015). Since the difference between T_R and T_A is considered to be the primary driving force of H (van der Tol et al., 2009), the modelled errors in H are expected to arise due to the uncertainties associated with T_R .

5.2 Canopy coupling, g_C and g_A versus transpiration and evaporation

The correlation analysis between $1-\Omega$ and λE_T revealed the extent of biophysical and radiative controls on λE_T (Fig. 5). The degree of biophysical control is a function of the ratio of g_C to g_A . Minor biophysical control on λE_T was apparent for forest and pasture during the wet seasons (Fig. 5c and 5d) as a result of a high g_C/g_A ratio along with increasing λE_T . Such conditions stimulate local humidification of air surrounding the canopy and uncoupling of the in-canopy vapor pressure deficit (D_0) from that in the air above (i.e., $D_0 < D_A$) (Meinzer et al., 1997; Motzer et al., 2005) (Fig. 9a), which implies that λE_T becomes largely independent of

g_C . On the contrary, an enhanced biophysical control on λE_T was apparent during the dry season and drought year 2005 during the period of reduced water supply particularly over PAS (Fig. 5e, 5f, and 7). Such condition leads to a relatively dry canopy surface, and substantially high g_A compared to g_C , thus resulting in low g_C/g_A ratios regardless of their absolute values (Meinzer et al., 1993; McNaughton and Jarvis, 1991). Here, fractional changes in g_C results in an equivalent fractional change in λE_T . This impedes transpiration from promoting local equilibrium of D_0 and minimizing (or maximizing) the gradient between D_0 and atmospheric vapor pressure deficit (D_A) (i.e., $D_0 \cong D_A$ or $D_0 > D_A$) (eqn. A10) (Fig 9a), thereby resulting in strong coupling between D_0 and D_A (Meinzer et al., 1993; Jarvis and McNaughton, 1986). Besides, a supplemental biophysical control on λE_T might have been imposed as a consequence of a direct negative feedback of D_A and D_0 on g_C (McNaughton and Jarvis, 1991; Jarvis, 1986). Increase in D_A (or D_0) beyond a certain limit decreases g_C (Fig. 7 and 8), resulting in a low and narrow increase of λE_T , despite steady increase in g_A and R_N . The combination of negative feedback response between D_A and g_C with the overall radiative-aerodynamic coupling significantly dampens the variation of transpiration in PAS and TDF in the dry season, thus featuring increased biophysical control in these PFTs. These results are in agreement with von Randow et al. (2012), who found enhanced biophysical control on λE_T for the pasture during the dry season. For the wet season, evidence of minor biophysical control indicates the dominance of R_N driven equilibrium evaporation in these PFTs (Hasler and Avissar, 2007; da Rocha et al., 2009; Costa et al., 2010). In the TRF and TMF, 94% and 99% of the retrieved g_C/g_A ratios fall above 0.5, and, only 1% and 6% of the retrieved g_C/g_A ratios fall below the 0.5 range (Fig. 9b). In contrast, 90% and 73% of the g_C/g_A ratios range above 0.5, and 10% to 27% of the g_C/g_A ratios were below 0.5 for TDF and PAS, respectively (Fig. 9b). This shows that, although radiation control is prevailing in all the sites, biophysical control is relatively

stronger in TDF and PAS as compared to the other sites. For large g_C/g_A ratios, the conditions within the planetary boundary layer (PBL) become decoupled from the synoptic scale (McNaughton and Jarvis, 1991) and the net radiative energy becomes the important regulator of transpiration. For small g_C/g_A ratios (e.g., in dry season), the conditions within the PBL are strongly coupled to the atmosphere above by rapid entrainment of air from the capping inversion and by some ancillary effects of sensible heat flux on the entrainment (McNaughton and Jarvis, 1991). These findings substantiate the earlier theory of McNaughton and Jarvis (1991), who postulated that large g_C/g_A ratios result in minor biophysical control on canopy transpiration due to the negative feedback on the canopy from the PBL. The negative relationship between $1-\Omega$ and λE_E (Fig. 5b) over all the PFTs is due to the feedback of g_A on g_C . However, over all the PFTs, a combined control of g_A and environmental variables on λE_E again highlighted the impact of realistically estimated g_A on λE_E (Holwerda et al., 2012).

It is important to mention that forests are generally expected to be better coupled to the atmosphere, which is related to generally higher g_A (due to high surface roughness) compared to the pastures.~~It is important to mention that forests are generally expected to be better coupled to the atmosphere, which is related to generally higher g_A/g_C ratios compared to the pastures.~~ This implies that forests exhibit stronger biophysical control on λE_T . However, due to the broad leaves of the rain forests (larger leaf area index) and higher surface wetness (due to higher rainfall amounts) the wet surface area is much larger in the forest than in the pastures. This results in much higher g_C values for forests than for pastures during the wet season ($g_C \approx g_A$), and $g_C/g_A \rightarrow 1$, and $g_C/g_A \rightarrow 1$. Consequently, no significant difference in coupling was found between them during the wet season (Fig. 5c and 5d). Despite the absolute differences in g_A and g_C between forest and pasture, the high surface wetness is largely offsetting the expected Ω difference between them. Although the surface wetness is

substantially lower during the dry season, the high water availability in the forests due to the deeper root systems help maintaining a relatively high g_C compared to the pastures. Hence, despite g_A (forest) $>$ g_A (pasture) during the dry season, substantially lower g_C values for the pasture result in lower g_C/g_A ratio for the pasture compared to the forest, thus causing more biophysical control on λE_T during the dry season. The relatively better relationship between coupling versus λE_T in PAS and TDF during the dry season was also attributed to high surface air temperature difference ($T_R - T_A$) in these PFTs that resulted in low g_C/g_A ratios (Fig. 9c).

5.3 Factors affecting g_C and g_A variability

The stomatal feedback-response hypothesis (Monteith, 1995) also became apparent at the canopy-scale (Fig. 8a, 8b), which states that a decrease in g_C with increasing D_A is caused by a direct increase in λE_T (Monteith, 1995; Matzner & Comstock, 2001; Streck, 2003) and g_C responds to the changes in the air humidity by sensing λE_T , rather than D_A . This feedback mechanism is found because of the influence of D_A on both g_C and λE_T , which in turn changes D_A by influencing the air humidity (Monteith, 1995). The change in g_C is dominated by an increase in the net available energy, which is partially offset by an increase in λE_T . After the net energy input in the canopy exceeds a certain threshold, g_C starts decreasing even if λE_T increases. High λE_T increases the water potential gradient between guard cells and other epidermal cells or reduces the bulk leaf water potential, thus causing stomatal closure (Monteith, 1995; Jones, 1998; Streck, 2003). The control of soil water on transpiration also became evident from the scatter plots between g_C versus λE_T and T_R for different D_A levels (Fig. 8b, 8c) (also Fig. 7). Denmead and Shaw (1962) hypothesized that reduced g_C and stomatal closure occurs at moderate to higher levels of soil moisture (high λE_T) when the atmospheric demand of water vapor increases (high D_A). The water content in the immediate

vicinity of the plant root depletes rapidly at high D_A , which decreases the hydraulic conductivity of soil, and the soil is unable to efficiently supply water under these conditions. For a given evaporative demand and available energy, transpiration is determined by the g_C/g_A ratio, which is further modulated by the soil water availability. These combined effects tend to strengthen the biophysical control on transpiration (Leuzinger and Kirner, 2010; Migletta et al., 2011). The complex interaction between g_C , T_R , and D_A (Fig. 8c) explains why different parametric g_C models produce divergent results.

Although λE_T and λE_E estimates are interdependent on g_C and g_A (as shown in Fig. 6 to Fig. 8); the figures reflect the credibility of the conductances as well as transpiration estimates by realistically capturing the hysteretic behavior between biophysical conductances and water vapor fluxes, which is frequently observed in natural ecosystems (Zhang et al., 2014, Renner et al., 2016). These results are also compliant with the theories postulated earlier from observations that the magnitude of hysteresis depends on the radiation-vapor pressure deficit time-lag, while the soil moisture availability is a key factor modulating the hysteretic transpiration-vapor pressure deficit relation as soil moisture declines (Zhang et al., 2014; O'Grady et al., 1999; Jarvis and McNaughton, 1986). This shows that despite being independent of any predefined hysteretic function, the interdependent conductance-transpiration hysteresis is still captured in STIC1.2.

Fig. 8d is in accordance with existing theory that under conditions of extremely high atmospheric turbulence (i.e., high g_A), a close coupling exists between the surface and the atmosphere, which causes T_R and T_A to converge (i.e., $T_R - T_A \rightarrow 0$). When g_A is low, the difference between T_R and T_A increases due to poor vertical mixing of the air.

6 Conclusions

By integrating the radiometric surface temperature (T_R) into a combined structure of PM-SW model we have estimated the canopy-scale biophysical conductances and quantified their

control on the terrestrial evapotranspiration components in a simplified SEB modeling perspective that treats the vegetation canopy as ‘big-leaf’. The STIC1.2 biophysical modeling scheme is independent of any leaf-scale empirical parameterisation for stomata and associated aerodynamic variables.

Stomata regulate the coupling between terrestrial carbon and water cycles, which implies that their behaviour under global environmental change is ~~critical~~decisive to predict vegetation functioning (Medlyn et al., 2011). The combination of variability in precipitation~~The combination of progressing rainfall reduction~~ (Hilker et al., 2014) and land cover change (Davidson et al., 2012) in the Amazon Basin is expected to increase the canopy-atmosphere coupling of pasture or forest systems under drier conditions by altering the ratio of the biological and aerodynamic conductances. An ~~I~~increase of biophysical control will most likely be an indicator of shifting the transpiration ~~pool~~ from an energy-limited to a water-limited regime (due to the impact of T_R , T_A , and D_A on the g_C/g_A ratio) with further consequences for the surface water balance and rainfall recycling. At the same time, a transition from forest to pasture or agriculture lands will substantially reduce the contribution of interception evaporation in the Amazon, hence, it will affect the regional water cycle. This might change the moisture regime of the Amazonian Basin and affect the moisture transport to other regions. STIC provides a new quantitative and internally consistent method for interpreting the biophysical conductances across a broad spectrum of PFTs in response to a range of climatic and ecohydrological conditions (excluding rising atmospheric CO_2). It could also provide the basis to improve existing land surface parameterisations for simulating vegetation water use at large spatial scales. However, it should also be noted that although the case study described here provides general insights into the biophysical controls of λE and associated feedback between g_C , D_A , T_R and λE_T in the framework of the PM equation, there is a tendency for overestimation of g_C ~~overestimation~~ due to the ~~entangling~~ embedded

evaporation information in the current single-source framework of STIC1.2. For accurate characterisation of canopy conductance, explicit partitioning of λE into transpiration and evaporation (both soil and interception) is one of the further scopes for improving STIC1.2 and this assumption needs to be tested further.

Acknowledgements

The developed modeling framework contributes to the "Catchments As Organized Systems (CAOS)" Phase-2 research group (FOR 1598) funded by the German Science Foundation (DFG) and to the "HiWET (High-resolution modelling and monitoring of Water and Energy Transfers in wetland ecosystems)" consortium funded by BELSPO and FNR. ~~This study was funded by the Luxembourg Institute of Science and Technology (LIST).~~ We sincere thank Dr. Andrew Jarvis (Lancaster University, UK), Dr. Monica Garcia (Technical University of Denmark, Denmark), and Dr. Georg Wohlfahrt (University of Innsbruck, Austria) for very helpful discussions and edits in the manuscript. We are grateful to all Brazilian and international collaborators and all the funding agencies that have contributed to the Large-scale Biosphere Atmosphere Experiment in Amazônia (LBA). The authors are indebted to Pavel Kabat, Antônio Ocimar Manzi, David R. Fitzjarrald, Julio Tota, Humberto Ribeiro da Rocha, Michael Goulden, Maarten J. Waterloo and Luiz Martinelli for planning, coordinating, conducting, and evaluating the eddy covariance, meteorological and leaf gas exchange measurements at the LBA sites. We are particularly grateful to all field technicians whose hard work were the key ingredients to establish the quality of the datasets used in this paper. The authors declare no conflict of interest. DTD acknowledges support of the Jet Propulsion Laboratory, California Institute of Technology, under a contract with the National Aeronautics and Space Administration.

Appendix:

A1 Derivation of 'state equations' in STIC 1.2

Neglecting horizontal advection and energy storage, the surface energy balance equation is written as follows:

$$\phi = \lambda E + H \quad (\text{A1})$$

Figure (A1) shows that, while H is controlled by a single aerodynamic resistance (r_A) (or $1/g_A$) the water vapor flux is controlled by two resistances in series, the surface resistance (r_C) (or $1/g_C$) and the aerodynamic resistance to vapor transfer ($r_C + r_A$). For simplicity, it is implicitly assumed that the aerodynamic resistance of water vapor and heat are equal (Raupach, 1998), and both the fluxes are transported from the same level from near surface to the atmosphere. The sensible and latent heat flux can be expressed in the form of aerodynamic transfer equations (Boegh et al., 2002; Boegh and Soegaard, 2004) as follows:

$$H = \rho c_P g_A (T_o - T_A) \quad (\text{A2})$$

$$\lambda E = \frac{\rho c_P}{\gamma} g_A (e_o - e_A) = \frac{\rho c_P}{\gamma} g_C (e_o^* - e_o) \quad (\text{A3})$$

Where T_o and e_o are the air temperature and vapor pressure at the source/sink height (i.e., aerodynamic temperature and vapor pressure) or at the so-called roughness length (z_o), where wind speed is zero. They represent the vapor pressure and temperature of the quasi-laminar boundary layer in the immediate vicinity of the surface level (Fig. A1), and T_o can be obtained by extrapolating the logarithmic profile of T_A down to z_o . e_o^* is the saturation vapor pressure at T_o (hPa).

By combining eqn. (A1), (A2), and (A3) and solving for g_A , we get the following equation.

$$g_A = \frac{\phi}{\rho c_P \left[(T_o - T_A) + \left(\frac{e_o - e_A}{\gamma} \right) \right]} \quad (\text{A4})$$

Combining the aerodynamic expressions of λE in eqn. (A3) and solving for g_C , we can express g_C in terms of g_A , e_0^* , e_0 , and e_A .

$$g_C = g_A \frac{(e_0 - e_A)}{(e_0^* - e_0)} \quad (\text{A5})$$

While deriving the expressions for g_A and g_C , two more unknown variables are introduced (e_0 and T_0), thus there are two equations and four unknowns. Therefore, two more equations are needed to close the system of equations.

An expression for T_0 is derived from the Bowen ratio (β) (Bowen, 1926) and evaporative fraction (Λ) (Shuttleworth et al., 1989) equation.

$$\beta = \left(\frac{1 - \Lambda}{\Lambda} \right) = \frac{\gamma(T_0 - T_A)}{(e_0 - e_A)} \quad (\text{A6})$$

$$T_0 = T_A + \left(\frac{e_0 - e_A}{\gamma} \right) \left(\frac{1 - \Lambda}{\Lambda} \right) \quad (\text{A7})$$

This expression for T_0 introduces another new variable (Λ); therefore, one more equation that describes the dependence of Λ on the conductances (g_A and g_C) is needed to close the system of equations. In order to express Λ in terms of g_A and g_C , we had adopted the advection – aridity (AA) hypothesis (Brutsaert and Stricker, 1979) with a modification introduced by (Mallick et al., 2015). The AA hypothesis is based on a complementary connection between the potential evaporation (E^*), sensible heat flux (H), and E ; and leads to an assumed link between g_A and T_0 . However, the effects of surface moisture (or water stress) were not explicit in the AA equation and Mallick et al. (2015) implemented a moisture constraint in the original advection-aridity hypothesis while deriving a ‘state equation’ of Λ (eqn. A8 below). A detailed derivation of the ‘state equation’ for Λ is described in the Supplement (S1) (also see Mallick et al., 2014, 2015). Estimation of e_0 , e_0^* , M , and α is described in the Appendix (A2).

$$\Lambda = \frac{2\alpha s}{2s + 2\gamma + \gamma \frac{g_A}{g_c}(1 + M)} \quad (A8)$$

A2 Iterative solution of e_0 , e_0^* , M , and α in STIC 1.2

Derivation of M

In STIC1.0 and 1.1 (Mallick et al., 2014; 2015), no distinction was made between the surface and source/sink height vapor pressures. Therefore, e_0^* was approximated as the saturation vapor pressure at T_R and e_0 was empirically estimated from M based on the assumption that the vapor pressure at the source/sink height ranges between extreme wet–dry surface conditions. However, the level of e_0 and e_0^* should be consistent with the level of the aerodynamic temperature (T_0) from which the sensible heat flux is transferred (Lhomme and Montes, 2014). The predictive use of the PM model could be hindered due to neglecting the feedbacks between the surface layer evaporative fluxes and source/sink height mixing and coupling (McNaughton and Jarvis, 1984), and their impact on the canopy scale conductances. Therefore, in STIC1.2, we have used physical expressions for estimating e_0 and e_0^* followed by estimating T_{SD} and M as described below. The fundamental differences between STIC1.0, 1.1 and 1.2 modeling philosophy is described in Table A1.

An estimate of e_0^* is obtained by inverting the aerodynamic transfer equation of λE .

$$e_0^* = e_A + \left[\frac{\gamma \lambda E (g_A + g_c)}{\rho c_P g_A g_c} \right] \quad (A9)$$

Following Shuttleworth and Wallace (1985) (SW85), the vapor pressure deficit (D_0) ($= e_0^* - e_0$) and vapor pressure (e_0) at the source/sink height are expressed as follows.

$$D_0 = D_A + \left[\frac{\{s\phi - (s + \gamma)\lambda E\}}{\rho c_P g_A} \right] \quad (A10)$$

$$e_0 = e_0^* - D_0 \quad (A11)$$

A physical equation of α is derived by expressing the evaporative fraction (Λ) as function of the aerodynamic equations of $H [\rho c_P g_A (T_0 - T_A)]$ and $\lambda E [\frac{\rho c_P}{\gamma} \frac{g_A g_C}{g_A + g_C} (e_0^* - e_A)]$ as follows.

$$\Lambda = \frac{\lambda E}{H + \lambda E} \quad (A12)$$

$$= \frac{\frac{\rho c_P}{\gamma} \frac{g_A g_C}{g_A + g_C} (e_0^* - e_A)}{\rho c_P g_A (T_0 - T_A) + \frac{\rho c_P}{\gamma} \frac{g_A g_C}{g_A + g_C} (e_0^* - e_A)} \quad (A13)$$

$$= \frac{g_C (e_0^* - e_A)}{[\gamma (T_0 - T_A) (g_A + g_C) + g_C (e_0^* - e_A)]} \quad (A14)$$

Combining eqn. (A14) and eqn. (A8) (eliminating Λ), we can derive a physical equation of α .

$$\alpha = \frac{g_C (e_0^* - e_A) \left[2s + 2\gamma + \gamma \frac{g_A}{g_C} (1 + M) \right]}{2s [\gamma (T_0 - T_A) (g_A + g_C) + g_C (e_0^* - e_A)]} \quad (A15)$$

Following Venturini et al. (2008), M can be expressed as the ratio of the vapor pressure difference to the vapor press deficit between surface to atmosphere as follows.

$$M = \frac{(e_0 - e_A)}{(e_0^* - e_A)} = \frac{(e_0 - e_A)}{\kappa (e_s^* - e_A)} = \frac{s_1 (T_{SD} - T_D)}{\kappa s_2 (T_R - T_D)} \quad (A16)$$

Where T_{SD} is the dewpoint temperature at source/sink height and T_D is the air dewpoint temperature; s_1 and s_2 are the psychrometric slopes of the saturation vapor pressure and temperature between $(T_{SD} - T_D)$ versus $(e_0 - e_A)$ and $(T_R - T_D)$ versus $(e_s^* - e_A)$ relationship (Venturini et al., 2008); and κ is the ratio between $(e_0^* - e_A)$ and $(e_s^* - e_A)$. Despite T_0 drives the sensible heat flux, the comprehensive dry-wet signature of underlying surface due to soil moisture variations is directly reflected in T_R (Kustas and Anderson, 2009). Therefore, using T_R in the denominator of eqn. (A16) tend to give a direct signature of the surface moisture

availability (M). In eqn. (A16), T_{SD} computation is challenging because both e_0 and s_l are unknown. By decomposing the aerodynamic equation of λE , T_{SD} can be expressed as follows.

$$\lambda E = \frac{\rho c_P}{\gamma} g_A (e_0 - e_A) = \frac{\rho c_P}{\gamma} g_A s_1 (T_{SD} - T_D)$$

$$T_{SD} = T_D + \frac{\gamma \lambda E}{\rho c_P g_A s_1} \quad (A17)$$

In the earlier STIC versions, s_l was approximated at T_D , e_0^* was approximated at T_R , T_{SD} was estimated from s_l , T_D , T_R , and related saturation vapor pressures (Mallick et al., 2014; 2015), and M was estimated from eqn. (A16) (estimation of T_{SD} and M was stand-alone earlier). However, since T_{SD} depends on λE and g_A , an iterative procedure is applied to estimate T_{SD} and M as described below.

In STIC1.2, an initial value of α is assigned as 1.26 and initial estimates of e_0^* and e_0 are obtained from T_R and M as $e_0^* = 6.13753e^{\frac{17.27T_R}{(T_R+237.3)}}$ and $e_0 = e_A + M(e_0^* - e_A)$. Initial T_{SD} and M were estimated as described above. With the initial estimates of these variables; first estimate of the conductances, T_0 , Λ , and λE are obtained. The process is then iterated by updating e_0^* (using eqn. A9), D_0 (using eqn. A10), e_0 (using eqn. A11), T_{SD} (using eqn. A17 with s_l estimated at T_D), M (using eqn. A16), and α (using eqn. A15), with the first estimates of g_C , g_A , and λE , and recomputing g_C , g_A , T_0 , Λ , and λE in the subsequent iterations with the previous estimates of e_0^* , e_0 , T_{SD} , M , and α until the convergence λE is achieved. Stable values of λE , e_0^* , e_0 , T_{SD} , M , and α are obtained within ~25 iterations. Illustrative examples of the convergence of e_0^* , e_0 , T_{SD} , M , and α are shown in Fig. (A3).

~~The retrieval of M is already described in Mallick et al. (2015) (as adopted from Venturini et al., 2008). We hypothesize that the moisture availability at the surface and at the evaporating front are uniform and, therefore, M is derived from the surface atmosphere information.~~

Following Venturini et al. (2008), M can be expressed as the ratio of the vapor pressure difference to the vapor press deficit between surface to atmosphere as follows:

$$M = \frac{(e_0 - e_A)}{(e_0^* - e_A)} = \frac{s_1(T_{SD} - T_D)}{s_2(T_0 - T_D)} \quad (A1)$$

Where T_{SD} is the dewpoint temperature of the evaporating front and T_D is the air dewpoint temperature, s_1 and s_2 are the psychrometric slopes of the saturation vapor pressure and temperature between $(T_{SD} - T_D)$ versus $(e_0 - e_A)$ and $(T_0 - T_D)$ versus $(e_0^* - e_A)$ relationship (Venturini et al., 2008). Since T_0 is not available and T_R and e_A are available, we compute s_2 as $s_2 = (e_s^* - e_A)/(T_R - T_D)$ with the assumption that errors due to any inequality between T_0 versus T_R and e_0^* versus e_s^* will be cancelled in this ratio. This appears to be a valid assumption due to the close relationship between T_0 and T_R (Huband and Monteith, 1986). In eq. A1, T_{SD} computation is challenging because both e_0 and s_1 are unknown. By decomposing the aerodynamic equation of λE , T_{SD} can be expressed as follows:

$$\lambda E = \frac{\rho c_P}{\gamma} g_A (e_0 - e_A) = \frac{\rho c_P}{\gamma} g_A s_1 (T_{SD} - T_D)$$

$$T_{SD} = T_D + \frac{\gamma \lambda E}{\rho c_P g_A s_1} \quad (A2)$$

In the earlier STIC versions, s_1 was approximated at T_D , T_{SD} was estimated from s_1 , T_D , T_R , and related saturation vapor pressures (Mallick et al., 2014; 2015), and M was estimated from eq. A1. However, since T_{SD} depends on λE and g_A , an iterative procedure is now applied to estimate T_{SD} and M as described below, which is another modification of the STIC1.0 and STIC1.1.

STIC1.2

In STIC1.0 and 1.1 (Mallick et al., 2014; 2015), no distinction was made between the surface and source/sink height vapor pressures. Therefore, e_0^* was approximated as the saturation vapor pressure at T_R and e_0 was empirically estimated from M based on the assumption that the vapor pressure at the source/sink height ranges between extreme wet-dry surface

conditions. However, the level of e_θ and e_θ^* should be consistent with the level of the aerodynamic temperature (T_θ) from which the sensible heat flux is transferred (Lhomme and Montes, 2014). The predictive use of the PM model could be hindered due to neglecting the feedbacks between the surface layer evaporative fluxes and source/sink height mixing and coupling (McNaughton and Jarvis, 1984), and their impact on the canopy scale conductances. Therefore, in STIC1.2, we have used physical expressions for estimating e_θ and e_θ^* followed by estimating T_{sD} and M as described below.

Following Shuttleworth and Wallace (1985) (SW85, hereafter), the vapor pressure deficit (D_θ) ($=e_\theta^* - e_\theta$) at the source/sink height is expressed as follows.

$$D_\theta = D_A + \left[\frac{\{s\phi - (s + \gamma)\lambda E\}}{\rho c_P g_A} \right] \quad (\text{A3})$$

An estimate of e_θ^* is obtained by inverting the aerodynamic transfer equation of λE .

$$e_\theta^* = e_A + \left[\frac{\gamma \lambda E (g_A + g_C)}{\rho c_P g_A g_C} \right] \quad (\text{A4})$$

A physical equation of α is derived by expressing the evaporative fraction (A) as function of the aerodynamic equations of $H [\rho c_P g_A (T_\theta - T_A)]$ and $\lambda E \left[\frac{\rho c_P g_A g_C}{\gamma g_A + g_C} (e_\theta^* - e_A) \right]$ as follows.

$$A = \frac{\lambda E}{H + \lambda E} \quad (\text{A5})$$

$$= \frac{\frac{\rho c_P g_A g_C}{\gamma g_A + g_C} (e_\theta^* - e_A)}{\rho c_P g_A (T_\theta - T_A) + \frac{\rho c_P g_A g_C}{\gamma g_A + g_C} (e_\theta^* - e_A)} \quad (\text{A6})$$

$$= \frac{g_C (e_\theta^* - e_A)}{[\gamma (T_\theta - T_A) (g_A + g_C) + g_C (e_\theta^* - e_A)]} \quad (\text{A7})$$

Combining eq. A7 and eq. 5, we can derive a physical expression of α as follows.

$$\alpha = \frac{g_e(e_g^* - e_A) \left[2s + 2\gamma + \gamma \frac{g_A}{g_e} (1 + M) \right]}{2s[\gamma(T_g - T_A)(g_A + g_e) + g_e(e_g^* - e_A)]} \quad (A8)$$

~~In STIC1.2, an initial value of α is assigned as 1.26 and initial estimates of e_{θ}^* and e_{θ} are obtained from T_R and M as $e_g^* = 6.13753e^{\frac{17.27T_R}{(T_R+237.3)}}$ and $e_g = e_A + M(e_g^* - e_A)$. Initial T_{SD} and M were estimated as described in the earlier section. With the initial estimates of these variables; first estimate of the conductances, T_{θ} , Λ , and λE are derived. The process is then iterated by updating D_{θ} (using eq. A3), e_{θ}^* (using eq. A4), e_{θ} ($e_{\theta} = e_{\theta}^* - D_{\theta}$), T_{SD} (using eq. A2 with s_L estimated at T_D), M [$M = s_L(T_{SD} - T_D)/s_2(T_R - T_D)$], and α (using eq. A8), with the first estimates of g_C , g_A , and λE , and recomputing g_A , g_C , T_{θ} , Λ , and λE in the subsequent iterations with the previous estimates of e_{θ}^* , e_{θ} , T_{SD} , M , and α until convergence of these variables is achieved. Stable values of e_{θ}^* , e_{θ} , T_{SD} , M , and α are obtained with ~25 iterations. Illustrative examples of the convergence of e_{θ}^* , e_{θ} , T_{SD} , M , and α are shown in Fig. A2.~~

To summarize, the computational steps of the conductances and evaporative fluxes in STIC are:

Step 1: Analytical solution of the conductances, T_{θ} and Λ by solving the ‘state equations’ (eqn. 2, 3, 4, and 5). Step 2: Initial estimates of the conductances (g_C and g_A), T_{θ} , Λ , λE and H . Step 3: Simultaneous iteration of λE , e_{θ}^ , e_{θ} , T_{SD} , M , and α ; and final estimation of the conductances (g_C and g_A), T_{θ} , Λ , λE and H . Step 4: Partitioning λE into λE_T and λE_E .*

References:

Andreae, M.O., Artaxo, P., Brandao, C., et al.: Biogeochemical cycling of carbon, water, energy, trace gases, and aerosols in Amazonia: The LBA-EUSTACH experiments, J. Geophys. Res., 107, D20, 8066, doi:10.1029/2001JD000524, 2002.

1494 Baker, I.T., Harper, A.B., da Rocha, H.R., Denning, A.S., et al.: Surface ecophysiological
 1495 behavior across vegetation and moisture gradients in tropical South America, *Agric. For.*
 1496 *Meteorol.*, 182– 183, 177– 188, 2013.

1497 Baldocchi, D.D., Wilson, K., and Gu, L.: How the environment, canopy structure and canopy
 1498 physiological functioning influence carbon, water and energy fluxes of a temperate
 1499 broad-leaved deciduous forest-An assessment with the biophysical model CANOAK,
 1500 *Tree Phys.*, 22(15–16), 1065, 2002.

1501 Baldocchi, D.D., and Ma, S.: How will land use affect air temperature in the surface
 1502 boundary layer? Lessons learned from a comparative study on the energy balance of an
 1503 oak savanna and annual grassland in California, USA, *Tellus B*, 65, 19994,
 1504 <http://dx.doi.org/10.3402/tellusb.v65i0.19994>, 2013.

1505 Ball, J.T., Woodrow, I.E., and Berry, J.A.: A model predicting stomatal conductance and its
 1506 contribution to the control of photosynthesis under different environmental conditions.
 1507 *In: Progress in Photosynthesis Research*, ed. J Biggins. M Nijhoff, Dordrecht, 4, 5.221-
 1508 5.224, Martinus-Nijhoff Publishers, Dordrecht, The Netherlands, 1987.

1509 Blyth, E., Gash, J., Lloyd, A., Pryor, M., Weedon, G.P., and Shuttleworth, W.J.: Evaluating
 1510 the JULES Land Surface Model Energy Fluxes Using FLUXNET Data, *J.*
 1511 *Hydrometeorol.*, 11, 509–519, doi: <http://dx.doi.org/10.1175/2009JHM1183.1>, 2010.

1512 Boegh, E., Soegaard, H., and Thomsen, A.: Evaluating evapotranspiration rates and surface
 1513 conditions using Landsat TM to estimate atmospheric resistance and surface resistance,
 1514 Remote Sens. Environ., 79, 329 – 343, 2002.

1515 Boegh, E., and Soegaard, H.: Remote sensing based estimation of evapotranspiration rates,
 1516 Int. J. Remote Sens., 25 (13), 2535 – 2551, 2004.

1517 Bonan, G.B., Williams, M., Fisher, R.A., and Oleson, K.W.: Modeling stomatal conductance
 1518 in the earth system: linking leaf water-use efficiency and water transport along the soil–

1519 plant–atmosphere continuum, *Geosci. Model Development*, 7, 2193–2222,
 1520 doi:10.5194/gmd-7-2193-2014, 2014.

1521 Bosveld, F.C., and Bouten, W.: Evaluating a model of evaporation and transpiration with
 1522 observations in a partially wet Douglas-fir forest, *Boundary Layer Meteorol.*, 108, 365 –
 1523 396, 2003.

1524 Boulet, G., Mougenot, B., Lhomme, J.-P., Fanise, P., Lili-Chabaane, Z., Olioso, A., Bahir,
 1525 M., Rivalland, V., Jarlan, L., Merlin, O., Coudert, B., Er-Raki, S., and Lagouarde, J.-P.:
 1526 The SPARSE model for the prediction of water stress and evapotranspiration
 1527 components from thermal infra-red data and its evaluation over irrigated and rainfed
 1528 wheat, *Hydrol. Earth Syst. Sci.*, 19, 4653-4672, doi:10.5194/hess-19-4653-2015, 2015.

1529 Bowen, I. S.: The ratio of heat losses by conduction and by evaporation from any water
 1530 surface, *Physics Rev.*, 27, 779–787, 1926.

1531 Brutsaert, W., and Stricker, H.: An advection-aridity approach to estimate actual regional
 1532 evapotranspiration, *Water Resour. Res.*, 15 (2), 443– 450, 1979.

1533 Chen, L., Zhang, Z., Li, Z., Tang, J., et al.: Biophysical control of whole tree transpiration
 1534 under an urban environment in Northern China, *J. Hydrol.*, 402, 388 – 400, 2011.

1535 Chen, F., and Schwerdtfeger, P.: Flux-gradient relationships for momentum and heat over a
 1536 rough natural surface. *Quar. J. Royal Met. Soc.*, 115, 335-352, 1989.

1537 Choudhury, B. J., and Monteith, J. L.: Implications of stomatal response to saturation deficit
 1538 for the heat balance of vegetation, *Agric. For. Meteorol.*, 36, 215 – 225, 1986.

1539 Christoffersen, B.O., Restrepo-Coupe, N., Arain, M.A., and Baker, I.T., et al.: Mechanisms of
 1540 water supply and vegetation demand govern the seasonality and magnitude of
 1541 evapotranspiration in Amazonia and Cerrado, *Agric. For. Meteorol.*, 191, 33 – 50, 2014.

1542 Colaizzi, P.D., Kustas, W.P., and Anderson, M.C., et al.: Two-source energy balance model
 1543 estimates of evapotranspiration using component and composite surface temperatures,
 1544 Adv. Water Resour., 50, 134-151, 2012.

1545 Contini, D., Donateo, A., and Belosi, F.: Accuracy of Measurements of Turbulent Phenomena
 1546 in the Surface Layer with an Ultrasonic Anemometer, J. Atm. Oceanic Tech., 23, 785–
 1547 801, doi: <http://dx.doi.org/10.1175/JTECH1881.1>, 2006.

1548 Costa, M.H., Biajoli, M.C., Sanches, L., Malhado, A.C.M. et al. : Atmospheric versus
 1549 vegetation controls of Amazonian tropical rain forest evapotranspiration: Are the wet
 1550 and seasonally dry rain forests any different?, J. Geophys. Res. – Biogeosci., 115,
 1551 G04021, doi: 10.1029/2009JG001179, 2010.

1552 Cox, P.M., Betts, R.A., Jones, C.D., Spall, S.A., and Totterdell, I.J.: Acceleration of global
 1553 warming due to carbon-cycle feedbacks in a coupled climate model, Nature, 408, 184 –
 1554 187, 2000.

1555 da Rocha, H.R., Manzi, A.O., Cabral, O.M. et al.: Patterns of water and heat flux across a
 1556 biome gradient from tropical forest to savanna in Brazil. J. Geophys. Res. – Biogeosci.,
 1557 114, G00B12, doi:10.1029/2007JG000640, 2009.

1558 da Rocha, H.R., Goulden, M., Miller, S., Menton, M., Pinto, L., Freitas, H., and Figueira,
 1559 A.S.: Seasonality of water and heat fluxes over a tropical forest in eastern Amazonia,
 1560 Ecol. Appl., 14(4), 22– 32, 2004.

1561 Davidson, E.A., de Araújo, A.C., Artaxo, P. et al.: The Amazon basin in transition, *Nature*,
 1562 481(7381), 321–328, 2012.

1563 Denmead, O.T., and Shaw, R.H.: Availability of soil water to plants as affected by soil
 1564 moisture content and meteorological conditions, Agron. J., 54, 385–390, 1962.

1565 Dolman, A.J., Miralles, D.G., and de Jeu, R.A.M.: Fifty years since Monteith's 1965 seminal
 1566 paper: the emergence of global ecohydrology, *Ecohydrol.*, 7, 897–902, doi:
 1567 10.1002/eco.1505, 2014.

1568 Drewry, D.T., Kumar, P., Long, S., Bernacchi, C., Liang, X.Z., and Sivapalan, M.:
 1569 Ecohydrological responses of dense canopies to environmental variability: 1. Interplay
 1570 between vertical structure and photosynthetic pathway, *J. Geophys. Res. – Biogeosci.*,
 1571 115, G04022, doi:10.1029/2010JG001340, 2010.

1572 Ershadi, A., et al.: Impact of model structure and parameterization on Penman–Monteith type
 1573 evaporation models, *J Hydrol.* 525, 521 – 535, 2015.

1574 Foken, T.: 50 Years of the Monin-Obukhov similarity theory, *Boundary-Layer Meteorol.*, 2,
 1575 7–29, 2006.

1576 Gatti, L.V., Gloor, M., Miller, J.B., et al.: Drought sensitivity of Amazonian carbon balance
 1577 revealed by atmospheric measurements, *Nature*, 506, 76–80, doi: 10.1038/nature12957,
 1578 2014.

1579 Gibson, L. A., Münch, Z., and Engelbrecht, J.: Particular uncertainties encountered in using a
 1580 pre-packaged SEBS model to derive evapotranspiration in a heterogeneous study area in
 1581 South Africa, *Hydrol. Earth Syst. Sci.*, 15, 295-310, doi:10.5194/hess-15-295-2011,
 1582 2011.

1583 Gloor, M., Brienen, R.J.W., Galbraith, D., et al.: Intensification of the Amazon hydrological
 1584 cycle over the last two decades, *Geophys. Res. Lett.*, 40, 1729–1733, 2013.

1585 de Goncalves, L.G.G., Borak, J.S., Costa, M.H., Saleska, S.R., et al.: Overview of the Large-
 1586 Scale Biosphere–Atmosphere Experiment in Amazonia Data Model Intercomparison
 1587 Project (LBA-DMIP), *Agric. For. Meteorol.*, 182– 183, 111– 127, 2013.

1588 Harper, A., Baker, I.T., Denning, A.S., Randall, D.A., Dazlich, D., and Branson, M.: Impact
 1589 of Evapotranspiration on Dry Season Climate in the Amazon Forest, *J. Climate*, 27, 574–
 1590 591, doi: <http://dx.doi.org/10.1175/JCLI-D-13-00074.1>, 2014.

1591 Hasler, N., and Avissar, R.: What controls evapotranspiration in the Amazon Basin, *J.*
 1592 *Hydrometeorol.*, 8, 380–395, doi: <http://dx.doi.org/10.1175/JHM587.1>, 2007.

1593 Hilker, T., Lyapustin, A.I., Tucker, C.J., et al.: Vegetation dynamics and rainfall sensitivity of
 1594 the Amazon, *Proc. National Academy of Sci.*, 111 (45), 16041 – 16046, doi:
 1595 10.1073/pnas.1404870111, 2014.

1596 Holwerda, F., Bruijnzeela, L.A., Scatenac, F.N., Vugtsa, H.F., and Meestersa, A.G.C.A.: Wet
 1597 canopy evaporation from a Puerto Rican lower montane rain forest: the importance of
 1598 realistically estimated aerodynamic conductance, *J. Hydrol.*, 414-415, 1-15, 2012.

1599 Huband, N.D.S., and Monteith, J.L.: Radiative surface temperature and energy balance of a
 1600 wheat canopy I: Comparison of radiative and aerodynamic canopy temperature,
 1601 *Boundary-Layer Meteorol.*, 36, 1-17, 1986.

1602 Huntingford, C., Fisher, R.A., Mercado, L., et al.: Towards quantifying uncertainty in
 1603 predictions of Amazon ‘dieback’, *Phil. Trans. Royal Soc. London. Ser. B, Biol. Sci.*, 363,
 1604 1857–1864, 2008.

1605 Jarvis, P. G.: The interpretation of leaf water potential and stomatal conductance found in
 1606 canopies in the field, *Philos. Trans. R. Soc. London B*, 273, 593–610, 1976.

1607 Jarvis, P.G.: Transpiration and assimilation of trees and agricultural crops: the ‘omega’
 1608 factor. In *Attributes of Trees and Crop Plants*, Edited by Cannell MGR and Jackson JE,
 1609 Institute of terrestrial Ecology, Edinburg, UK, 460 – 480, 1986.

1610 Jarvis, P.G., and McNaughton, K.G.: Stomatal control of transpiration: scaling up from leaf
 1611 to region, *Adv. Ecol. Res.*, 15, 1 – 49, 1986.

1612 Jones, H.G.: Stomatal control of photosynthesis and transpiration, J. Exp. Bot., 49, 387 – 398,
 1613 1998.

1614 [Kumagai, T., et al.: Transpiration, canopy conductance and the decoupling coefficient of a](#)
 1615 [lowland mixed dipterocarp forest in Sarawak, Borneo: dry spell effects, J. Hydrol., 287,](#)
 1616 [237–251, 2004.](#)

1617 [Kustas, W.P., and Anderson, M.C.: Advances in thermal infrared remote sensing for land](#)
 1618 [surface modeling, Agric. For. Meteorol., 149, 2071 – 2081, 2009.](#)

1619 Lawrence, D., and Vandecar, K.: Effects of tropical deforestation on climate and agriculture,
 1620 Nature Clim. Change, 5, 27–36, doi: 10.1038/nclimate2430, 2015.

1621 Leuning, R.: A critical appraisal of a combined stomatal – photosynthesis model for c3
 1622 plants, Pl. Cell and Environ., 18, 339 – 355, 1995.

1623 Leuzinger, S., and Kirner, C.: Rainfall distribution is the main driver of runoff under future
 1624 CO₂-concentration in a temperate deciduous forest, Global Change Biol., 16, 246 – 254,
 1625 2010.

1626 Lhomme, J.P., and Montes, C.: Generalized combination equations for canopy evaporation
 1627 under dry and wet conditions, Hydrol. Earth Sys. Sci., 18, 1137–1149, 2014.

1628 Loescher, H.W., Gholz, H.L., Jacobs, J.M., and Oberbauer, S.F.: Energy dynamics and
 1629 modeled evapotranspiration from a wet tropical forest in Costa Rica, J. Hydrol., 315, 274
 1630 – 294, 2005.

1631 [Ma, N., et al.: Environmental and biophysical controls on the evapotranspiration over the](#)
 1632 [highest alpine steppe, J. Hydrol., 529 \(3\), 980–992, 2015.](#)

1633 Malhi, Y., Pegoraro, E., Nobre, A.D., Pereira, M.G.P., Grace, J., Culf, A.D., and Clement, R.:
 1634 The energy and water dynamics of a central Amazonian rain forest, J. Geophys. Res.,
 1635 107, D20, 10.1029/2001JD000623, 2002.

1636 Malhi, Y.: The productivity, metabolism and carbon cycle of tropical forest vegetation, J.
 1637 Ecol., 100, 65–75, 2012.

1638 Mallick, K., Boegh, E., Trebs, I., et al.: Reintroducing radiometric surface temperature into
 1639 the Penman-Monteith formulation, Water Resour. Res., 51,
 1640 doi:10.1002/2014WR016106, 2015.

1641 Mallick, K., Jarvis, A.J., Boegh, E., et al.: A surface temperature initiated closure (STIC) for
 1642 surface energy balance fluxes, Remote Sens. Environ., 141, 243 – 261, 2014.

1643 [Massman, W. J.: A model study of \$kB_H^{-1}\$ for vegetated surfaces using 'localized near-field'](#)
 1644 [Lagrangian theory, J. Hydrol., 223, 27-43, 1999.](#)

1645 Miglietta, F., Peressotti, A., Viola, R., Körner, C., and Amthor, J.S.: Stomatal numbers, leaf
 1646 and canopy conductance, and the control of transpiration, Proc. National Acad. Sci., 108
 1647 (28), E275-E275, 2011.

1648 Matheny, A.M., Bohrer, G., Stoy, P., Baker, I.T., et al.: Characterizing the diurnal patterns of
 1649 errors in the prediction of evapotranspiration by several land-surface models: An NACP
 1650 analysis, J. Geophys. Res.- Biogeosci., 119, doi:10.1002/2014JG002623, 2014.

1651 Matzner, S., and Comstock, J.: The temperature dependence of shoot hydraulic resistance:
 1652 implications for stomatal behaviour and hydraulic limitation, Pl. Cell and Environ., 24
 1653 (11), 1299 – 1307, 2001.

1654 McNaughton, K.G., and Jarvis, P.G.: Using the Penman-Monteith equation predictively,
 1655 Agric. Water Management, 8 (1-3), 263-278, 1984.

1656 McNaughton, K.G., and Jarvis, P.G.: Effects of spatial scale on stomatal control of
 1657 transpiration, Agric. For. Meteorol., 54, 279 – 301, 1991.

1658 Medlyn, B.E., Duursma, R.A., Eamus, D., et al.: Reconciling the optimal and empirical
 1659 approaches to modelling stomatal conductance, *Global Change Biol.*, doi:
 1660 10.1111/j.1365-2486.2010.02375.x, 2011.

1661 Meinzer, F.C., Andrade, J.L., Goldstein, G., Holbrook, N.M., Cavelier, J., and Jackson, P.:
 1662 Control of transpiration from upper canopy of a tropical forest: the role of stomatal,
 1663 boundary layer and hydraulic architecture components, *Pl. Cell and Environ.*, 20, 1242 –
 1664 1252, 1997.

1665 Meinzer, F.C., Goldstein, G., Holbrook, N.M., Jackson, P., Cavelier, J.: Stomatal and
 1666 environmental control of transpiration in a lowland tropical forest site, *Pl. Cell and*
 1667 *Environ.*, 16, 429 – 436, 1993.

1668 Mercado, L.M., Lloyd, J., Dolman, A.J., Sitch, S., and Pati, S.: Modelling basin-wide
 1669 variations in Amazon forest productivity – Part 1: Model calibration, evaluation and
 1670 upscaling functions for canopy photosynthesis, *Biogeosci.*, 6, 1247-1272, doi:
 1671 10.5194/bg-6-1247-2009, 2009.

1672 Monteith, J.L.: Evaporation and environment. In G.E. Fogg (ed.) *Symposium of the Society*
 1673 *for Experimental Biology, The State and Movement of Water in Living Organisms*, 19,
 1674 pp. 205-234. Academic Press, Inc., NY, 1965.

1675 Monteith, J.L.: Evaporation and surface temperature, *Quart. J. Royal Met. Soc.*, 107, 1–27,
 1676 1981.

1677 Monteith, J.L.: Accommodation between transpiring vegetation and the convective boundary
 1678 layer, *J. Hydrol.*, 166, 251 – 263, 1995.

1679 Monteith, J.L., and Unsworth, M.H.: *Principles of Environmental Physics*. Elsevier,
 1680 Amsterdam, 2008.

1681 Moran, M.S., Clarke, T.R., Inoue, Y., Vidal, A.: Estimating crop water deficit between
 1682 surface-air temperature and spectral vegetation index, *Remote Sens. Environ.*, 46, 246-
 1683 263, 1994.

1684 Motzer, T., Munz, N., Kupperts, M., Schmitt, D., and Anhuf, D.: Stomatal conductance,
 1685 transpiration and sap flow of tropical montane rain forest trees in the southern
 1686 Ecuadorian Andes, *Tree Physiol.*, 25, 1283 – 1293, 2005.

1687 O’Grady, A.P., Eamus, D., and Hutley, L. B.: Transpiration increases during the dry season:
 1688 patterns of tree water use in eucalypt open-forests of northern Australia, *Tree Physiol.*,
 1689 19, 591—597, 1999.

1690 Penman, H.L.: Natural evaporation from open water, bare soil, and grass, *Proc. Royal Soc.*
 1691 London, Ser. A, 193, 120–146, 1948.

1692 Priante Filho, N., Vourlitis, G.L., Hayashi, M.M.S., de Souza Nogueira, J., et al.: Comparison
 1693 of the mass and energy exchange of a pasture and a mature transitional tropical forest of
 1694 the southern Amazon Basin during a seasonal transition, *Global Change Biol.*, 10, 863–
 1695 876, doi: 10.1111/j.1529-8817.2003.00775.x, 2004.

1696 Priestley, C.H.B., and Taylor, R.J.: On the assessment of surface heat flux and evaporation
 1697 using large scale parameters, *Monthly Weather Rev.*, 100, 81–92, 1972.

1698 Prihodko, L., Denning, A.S., Hanan, N.P., Baker, I.T., and Davis, K.: Sensitivity, uncertainty
 1699 and time dependence of parameters in a complex land surface model, *Agric. For.*
 1700 *Meteorol.*, 148 (2), 268–287, 2008.

1701 Raupach, M.R.: Vegetation-atmosphere interaction and surface conductance at leaf, canopy
 1702 and regional scales, *Agric. For. Meteorol.*, 73, 151-179, 1995.

1703 Raupach, M.R., and Finnigan, J.J.: Scale issues in boundary-layer meteorology: surface
 1704 energy balance in heterogeneous terrain, *Hydrol. Proc.*, 9, 589 – 612, 1995.

Raupach, M.R.: Influence of local feedbacks on land-air exchanges of energy and carbon, Global Change Biol., 4, 477 – 494, 1998.

Renner, M., Hassler, S.K., Blume, T., Weiler, M., et al.: Dominant controls of transpiration along a hillslope transect inferred from ecohydrological measurements and thermodynamic limits, Hydrol. Earth Syst. Sci., 20, 2063-2083, doi:10.5194/hess-20-2063-2016, 2016.

Richiardone, R., Manfrin, M., Ferrarese, S., Francone, C., Fernicola, V., Gavioso, R.M., and Mortarini, L.: Influence of the Sonic Anemometer Temperature Calibration on Turbulent Heat-Flux Measurements, Boundary Layer Meteorol., 142 (3), 425-442, 2012.

Roy, S.B., and Avissar, R.: Impact of land use/land cover change on regional hydrometeorology in Amazonia, J. Geophys. Res., 107, D20, doi: 10.1029/2000JD000266, 2002.

Natalia Restrepo-Coupea, N., da Rocha, H.R., Hutrya, L.R., da Araujo, A.C., et al.: What drives the seasonality of photosynthesis across the Amazon basin? A cross-site analysis of eddy flux tower measurements from the Brasil flux network, Agric. For. Meteorol., 182– 183, 128– 144, 2013.

Ocheltree, T.W., Nippert, J.B., and Prasad, P.V.V.: Stomatal responses to changes in vapor pressure deficit reflect tissue-specific differences in hydraulic conductance, Pl. Cell Environ., 37, 132–139, 2014.

Saleska, S.R., da Rocha, H.R., Huete, A.R., Nobre, A.D., Artaxo, P., and Shimabukuro, Y.E.: LBA-ECO CD-32 Flux Tower Network Data Compilation, Brazilian Amazon: 1999-2006. Data set. Available on-line [http://daac.ornl.gov] from Oak Ridge National Laboratory Distributed Active Archive Center, Oak Ridge, Tennessee, USA, <http://dx.doi.org/10.3334/ORNLDAAAC/1174>, 2013.

1729 [Shuttleworth, W. J., Gurney, R. J., Hsu, A. Y., and Ormsby, J. P.: FIFE: The variation in](#)
 1730 [energy partition at surface flux sites, in Remote Sensing and Large Scale Processes,](#)
 1731 [Proceedings of the IAHS Third International Assembly, vol. 186, edited by A. Rango,](#)
 1732 [pp. 67–74, IAHS Publ., Baltimore, Md, 1989.](#)
 1733 Shuttleworth, W.J.: Micrometeorology of temperate and tropical forest, Phil. Trans. Royal
 1734 Soc. London. Ser. B, Biol. Sci., 324, 299-334, 1989.
 1735 Shuttleworth, W.J.: Putting the "vap" into evaporation. Hydrol. Earth Sys. Sci., 11, 210-244,
 1736 doi: 10.5194/hess-11-210-2007, 2007.
 1737 Shuttleworth, W.J., and Wallace, J.S.: Evaporation from sparse crops – an energy
 1738 combination theory, Quart. J. Royal Met. Soc., 111, 839 – 855, 1985.
 1739 [Simpson, I.J., Thurtell, G.W., Nuemann, H.H., den Hartog, G., Edwards, G.C.: The validity](#)
 1740 [of similarity theory in the roughness sublayer above forests, Boundary- Layer](#)
 1741 [Meteorology 87, 69-99, 1998.](#)
 1742 [Stella, P., Kortner, M., Ammann, C., Foken, T., Meixner, F. X., and Trebs, I.: Measurements](#)
 1743 [of nitrogen oxides and ozone fluxes by eddy covariance at a meadow: evidence for an](#)
 1744 [internal leaf resistance to NO₂, Biogeosci., 10, 5997-6017, doi:10.5194/bg-10-5997-](#)
 1745 [2013, 2013.](#)
 1746 Streck, N.A.: Stomatal response to water vapor pressure deficit: an unsolved issue, Revista
 1747 Brasil. Agrociên., 9 (4), 317–322, 2003.
 1748 [Thom, A.S., Stewart, J.B., Oliver, H.R., Gash, J.H.C.: Comparison of aerodynamic and](#)
 1749 [energy budget estimates of fluxes over a pine forest, Quart. J. Royal Met. Soc., 101, 93-](#)
 1750 [105, 1975.](#)
 1751 Tuzet, A., Perrier, A., and Leuning, R.: A coupled model of stomatal conductance,
 1752 photosynthesis and transpiration, Pl. Cell Environ., 26, 1097–1116, 2003.

- van der Tol, C., van der Tol, S., Verhoef, A., Su, B., Timmermans, J., Houldcroft, C., and Gieske, A.: A Bayesian approach to estimate sensible and latent heat over vegetated land surface, *Hydrol. Earth Sys. Sci.*, 13, 749–758, doi:10.5194/hess-13-749-2009, 2009.
- Van Dijk, A.I.J.M., et al.: Rainfall interception and the couple surface water and energy balance, *Agric. For. Meteorol.*, 214 – 215, 402 – 415, 2015.
- Venturini, V., Islam, S., and Rodriguez, L.: Estimation of evaporative fraction and evapotranspiration from MODIS products using a complementary based model, *Remote Sens. Environ.*, 112(1), 132-141, 2008.
- von Randow, R.C.S., von Randow, C., Hutjes, R.W.A., Tomasella, J., and Kruijt, B.: Evapotranspiration of deforested areas in central and southwestern Amazonia, *Theor. Appl. Climatol.*, 109:205–220, doi: 10.1007/s00704-011-0570-1, 2012.
- Villagarcía, L., Were, A., García, M., and Domingo, F.: Sensitivity of a clumped model of evapotranspiration to surface resistance parameterisations: Application in a semi-arid environment, *Agric. For. Meteorol.*, 150 (7), 1065-1078, 2010.
- Villani, M.G., Schmid, H.P., Su, H.B., Hutton, J.L., and Vogel, C.S.: Turbulence statistics measurements in a northern hardwood forest, *Boundary-Layer Meteorology* 108: 343–364, 2003.
- Zhang, Q., Manzoni, S., Katul, G., Porporato, A., and Yang, D.: The hysteretic evapotranspiration-vapor pressure deficit relation, *J. Geophys. Res. Biogeosci.*, 119, 125–140, doi:10.1002/2013JG002484, 2014.

Table 1: Variables and symbols and their description used in the study

<u>Variables and symbol</u>	<u>Description</u>
λE	Evapotranspiration (evaporation + transpiration) as latent heat flux (W m^{-2})
H	Sensible heat flux (W m^{-2})
R_N	Net radiation (W m^{-2})
G	Ground heat flux (W m^{-2})
ϕ	Net available energy (W m^{-2})
T_A	Air temperature ($^{\circ}\text{C}$)
T_D	Dewpoint temperature ($^{\circ}\text{C}$)
T_R	Radiometric surface temperature ($^{\circ}\text{C}$)
R_H	Relative humidity (%)
e_A	Atmospheric vapor pressure at the level of T_A measurement (hPa)
D_A	Atmospheric vapor pressure deficit at the level of T_A measurement (hPa)
W_S	Wind speed (m s^{-1})
u^*	Friction velocity (m s^{-1})
T_{SD}	Dew-point temperature at the source/sink height ($^{\circ}\text{C}$)
T_0	Aerodynamic surface temperature or source/sink height temperature ($^{\circ}\text{C}$)
e_s	‘effective’ vapor pressure of evaporating front near the surface (hPa)
e_s^*	Saturation vapor pressure of surface (hPa)
e_0^*	Saturation vapor pressure at the source/sink height (hPa)
e_0	Atmospheric vapor pressure at the source/sink height (hPa)
D_0	Atmospheric vapor pressure deficit at the source/sink height (hPa)
λE_{eq}	Equilibrium latent heat flux (W m^{-2})
λE_{imp}	Imposed latent heat flux (W m^{-2})
λE_E	Evaporation as flux (W m^{-2})
λE_T	Transpiration flux (W m^{-2})
E	Evapotranspiration (evaporation + transpiration) as depth of water (mm)
λE^*	Potential evaporation as flux (W m^{-2})
λE_T^*	Potential transpiration as flux (W m^{-2})
λE_W	Wet environment evaporation as flux (W m^{-2})
λE_P^*	Potential evaporation as flux according to Penman (W m^{-2})
λE_{PM}^*	Potential evaporation as flux according to Penman-Monteith (W m^{-2})
λE_{PT}^*	Potential evaporation as flux according to Priestley-Taylor (W m^{-2})
E^*	Potential evaporation as depth of water (mm)
E_P^*	Potential evaporation as depth of water according to Penman (mm)
E_{PM}^*	Potential evaporation as depth of water according to Penman-Monteith (mm)
E_{PT}^*	Potential evaporation as depth of water according to Priestley-Taylor (mm)
E_W	Wet environment evaporation as depth of water (mm)
g_A	Aerodynamic conductance (m s^{-1})
g_C	Stomatal / surface conductance (m s^{-1})
g_M	Momentum conductance (m s^{-1})
g_B	Quasi-laminar boundary layer conductance (m s^{-1})
g_{Smax}	Maximum stomatal / surface conductance (m s^{-1}) ($= g_S/M$)

<u>M</u>	Surface moisture availability (0 – 1)
<u>s</u>	Slope of saturation vapor pressure versus temperature curve (hPa K^{-1}) (estimated at T_A)
<u>s_1</u>	Slope of the saturation vapor pressure and temperature between ($T_{SD} - T_D$) versus ($e_0 - e_A$) (approximated at T_D) (hPa K^{-1})
<u>s_2</u>	Slope of the saturation vapor pressure and temperature between ($T_R - T_D$) versus ($e_s^* - e_A$) (hPa K^{-1})
<u>s_3</u>	Slope of the saturation vapor pressure and temperature between ($T_R - T_{SD}$) versus ($e_s^* - e_s$) (approximated at T_R) (hPa K^{-1})
<u>κ</u>	Ratio between ($e_0^* - e_A$) and ($e_s^* - e_A$)
<u>λ</u>	Latent heat of vaporization of water ($\text{J kg}^{-1} \text{K}^{-1}$)
<u>z_R</u>	Reference height (m)
<u>z_M</u>	Effective source-sink height of momentum (m)
<u>z_0</u>	Roughness length (m)
<u>d</u>	Displacement height (m)
<u>γ</u>	Psychrometric constant (hPa K^{-1})
<u>ρ</u>	Density of air (kg m^{-3})
<u>c_p</u>	Specific heat of dry air ($\text{MJ kg}^{-1} \text{K}^{-1}$)
<u>Δ</u>	Evaporative fraction (unitless)
<u>β</u>	Bowen ratio (unitless)
<u>α</u>	Priestley-Taylor parameter (unitless)
<u>Ω</u>	Decoupling coefficient (unitless)
<u>S_c</u>	Schmidt number (unitless)
<u>P_r</u>	Prandtl number (unitless)
<u>k</u>	Von Karman's constant (0.4)

1778

1779

1780

1781

1782

1783

1784

1785

1786

1787

1788

Table 12. Overview of the LBA tower sites.

Biome	PFT	Site	LBA Code	Data availability period	Latitude	Longitude	Tower height (m)	Annual rainfall (mm)
Forest	Tropical rainforest (TRF)	Manaus KM34	K34	06/1999 to 09/2006	-2.609	-60.209	50	2329
Forest	Tropical moist forest (TMF)	Santarem KM67	K67	01/2002 to 01/2006	-2.857	-54.959	63	1597
Forest	Tropical moist forest (TMF)	Santarem KM83	K83	07/2000 to 12/2004	-3.018	-54.971	64	1656
Forest	Tropical dry forest (TDF)	Reserva Biológica Jarú	RJA	03/1999 to 10/2002	-10.083	-61.931	60	2354
Pasture	Pasture (PAS)	Santarem KM77	K77	01/2000 to 12/2001	-3.012	-54.536	18	1597
Pasture	Pasture (PAS)	Fazenda Nossa Senhora	FNS	03/1999 to 10/2002	-10.762	-62.357	8.5	1743

Table 23. Comparative statistics for the STIC and tower-derived hourly g_A and g_C for a range of PFTs in the Amazon Basin (LBA tower sites). Values in parenthesis are \pm one standard deviation (standard error for correlation).

PFTs	$g_A\text{-STIC}$ vs. $g_A\text{-BM13}$					$g_C\text{-STIC}$ vs. $g_C\text{-INV}$			
	RMSD (m s^{-1})	R^2	Slope	Offset (m s^{-1})	N	RMSD (m s^{-1})	R^2	Slope	Offset (m s^{-1})
TRF	0.013	0.41 (± 0.03)	1.07 (± 0.047)	0.0031 (± 0.0008)	1159	0.012	0.14 (± 0.04)	0.39 (± 0.039)	0.0097 (± 0.0007)
TMF	0.012	0.55 (± 0.12)	0.81 (± 0.023)	0.0006 (± 0.0006)	1927	0.009	0.55 (± 0.12)	0.85 (± 0.025)	0.0032 (± 0.0005)
TDF	0.007	0.49 (± 0.15)	0.89 (± 0.041)	0.0019 (± 0.0006)	787	0.012	0.33 (± 0.19)	0.30 (± 0.022)	0.0050 (± 0.0005)
PAS	0.012	0.22 (± 0.18)	1.03 (± 0.083)	0.0059 (± 0.0007)	288	0.007	0.58 (± 0.12)	0.65 (± 0.025)	0.0024 (± 0.0003)
Mean	0.012	0.44 (± 0.10)	0.76 (± 0.016)	0.0047 (± 0.003)	4161	0.010	0.39 (± 0.08)	0.63 (± 0.016)	0.0046 (± 0.0003)

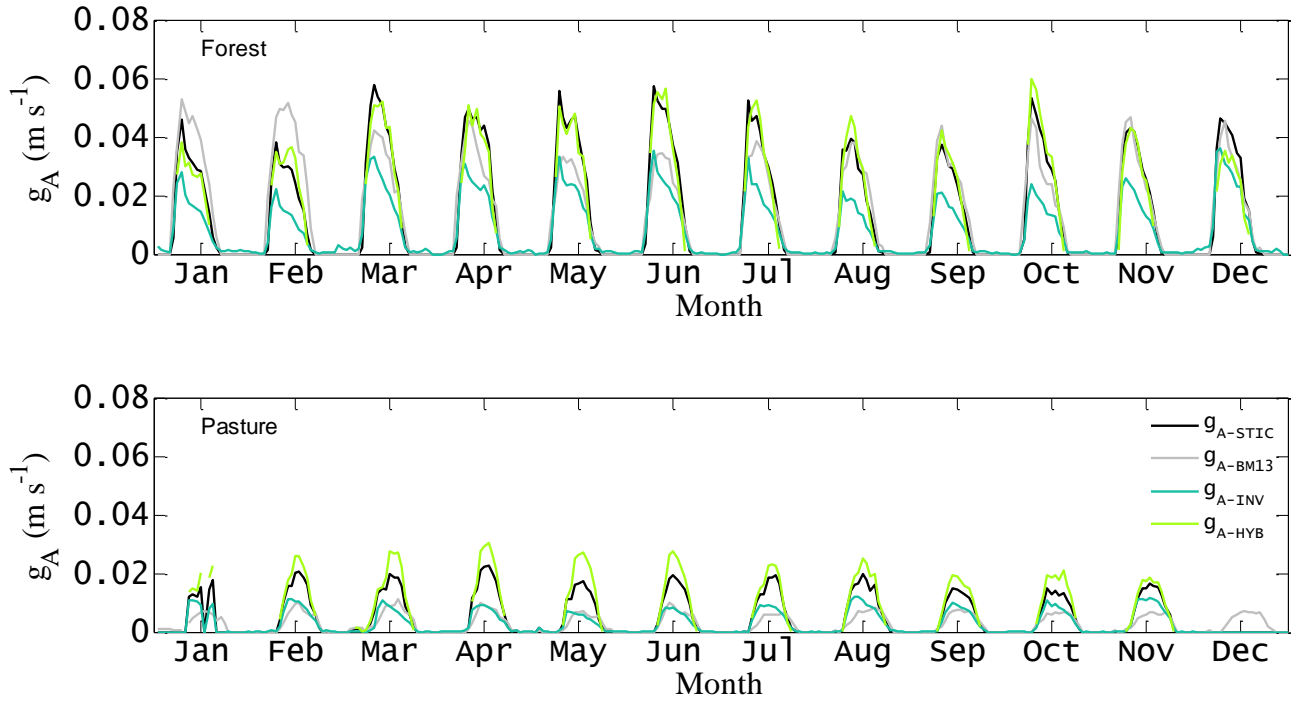
N = number of data points; RMSD = root mean square deviation between predicted (P) and observed (O) variables = $\left[\frac{1}{N} \sum_{i=0}^N (P_i - O_i)^2 \right]^{1/2}$.

Table 34. Comparative statistics for the STIC and tower-derived hourly λE and H for a range of PFTs in the Amazon Basin (LBA tower sites). Values in parenthesis are \pm one standard deviation (standard error for correlation).

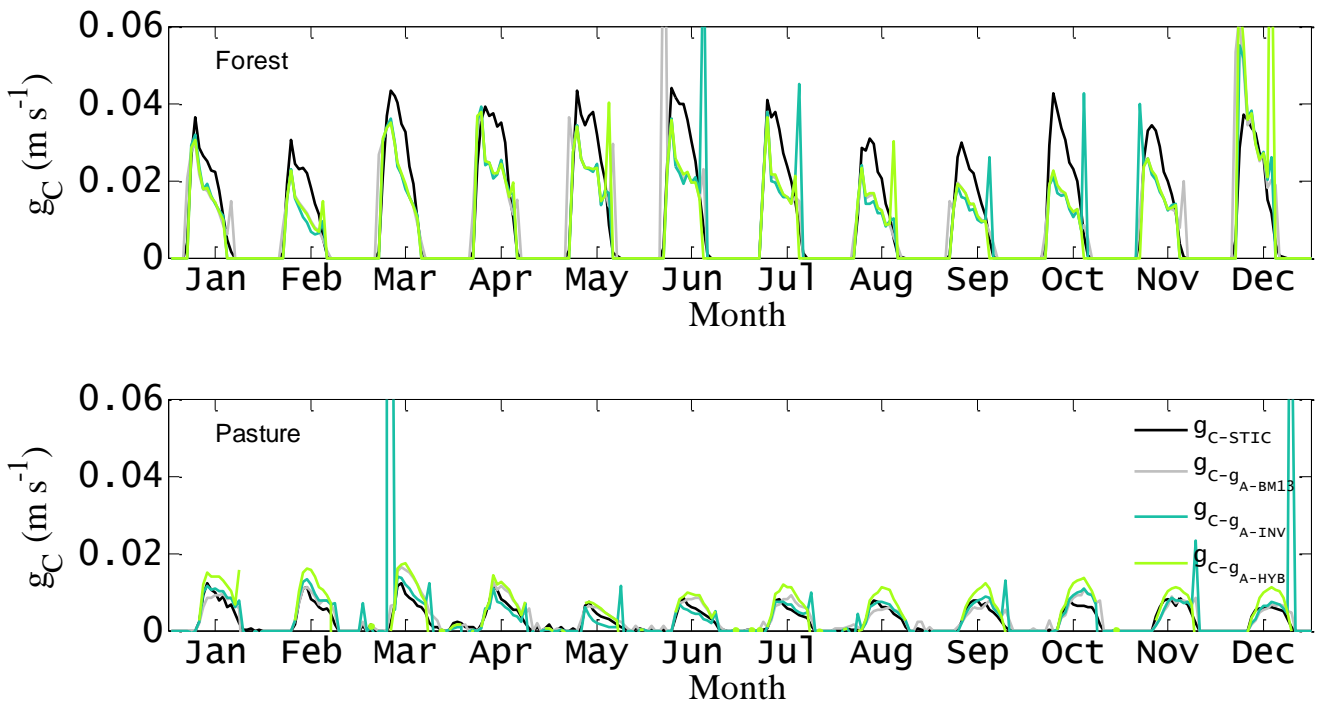
PFTs	λE				H				
	RMSD (W m ⁻²)	R ²	Slope	Offset (W m ⁻²)	RMSD (W m ⁻²)	R ²	Slope	Offset (W m ⁻²)	N
TRF	28	0.96 (± 0.007)	1.10 (± 0.008)	-16 (± 2)	34	0.52 (± 0.030)	0.60 (± 0.025)	29 (± 2)	1159
TMF	20	0.98 (± 0.004)	1.08 (± 0.004)	-11 (± 1)	23	0.71 (± 0.019)	0.61 (± 0.014)	20 (± 1)	1927
TDF	26	0.96 (± 0.009)	0.96 (± 0.008)	-7 (± 2)	30	0.66 (± 0.032)	0.89 (± 0.035)	20 (± 3)	787
PAS	31	0.96 (± 0.009)	1.14 (± 0.010)	-2 (± 2)	33	0.88 (± 0.016)	0.67 (± 0.011)	9 (± 1)	288
Mean	33	0.94 (± 0.005)	1.04 (± 0.005)	-1 (± 1)	37	0.61 (± 0.021)	0.58 (± 0.009)	24 (± 2)	4161

1819 **Figure 1.** Examples of monthly averages of the diurnal time series of canopy-scale (a) g_A and (b) g_C
1820 estimated for two different biomes (forest and pasture) in the Amazon Basin (LBA sites K34 and
1821 FNS). The time series of four different g_A estimates and their corresponding g_C estimates are shown
1822 here.

(a) Time series g_A



(b) Time series g_C



1823

1824 **Figure 2.** (a) Comparison between STIC derived g_A (g_{A-STIC}) with an estimated aerodynamic
1825 conductance based on friction velocity (u^*) and wind speed (u) according to Baldocchi and Ma (2013)
1826 (g_{A-BM13}), (b) Comparison between g_{A-STIC} with an inverted g_A (g_{A-INV}) based on EC observations of λE
1827 and D_A , (c) Comparison between g_{A-STIC} with a hybrid g_A (g_{A-HYB}) based on EC observations of H and
1828 estimated T_0 over the LBA EC sites, (d) Comparison between residual g_A differences versus u and u^* ,
1829 (e) and (f) Relationship between wind and shear derived g_A versus ϕ , T_R , and D_A over the LBA EC
1830 sites.

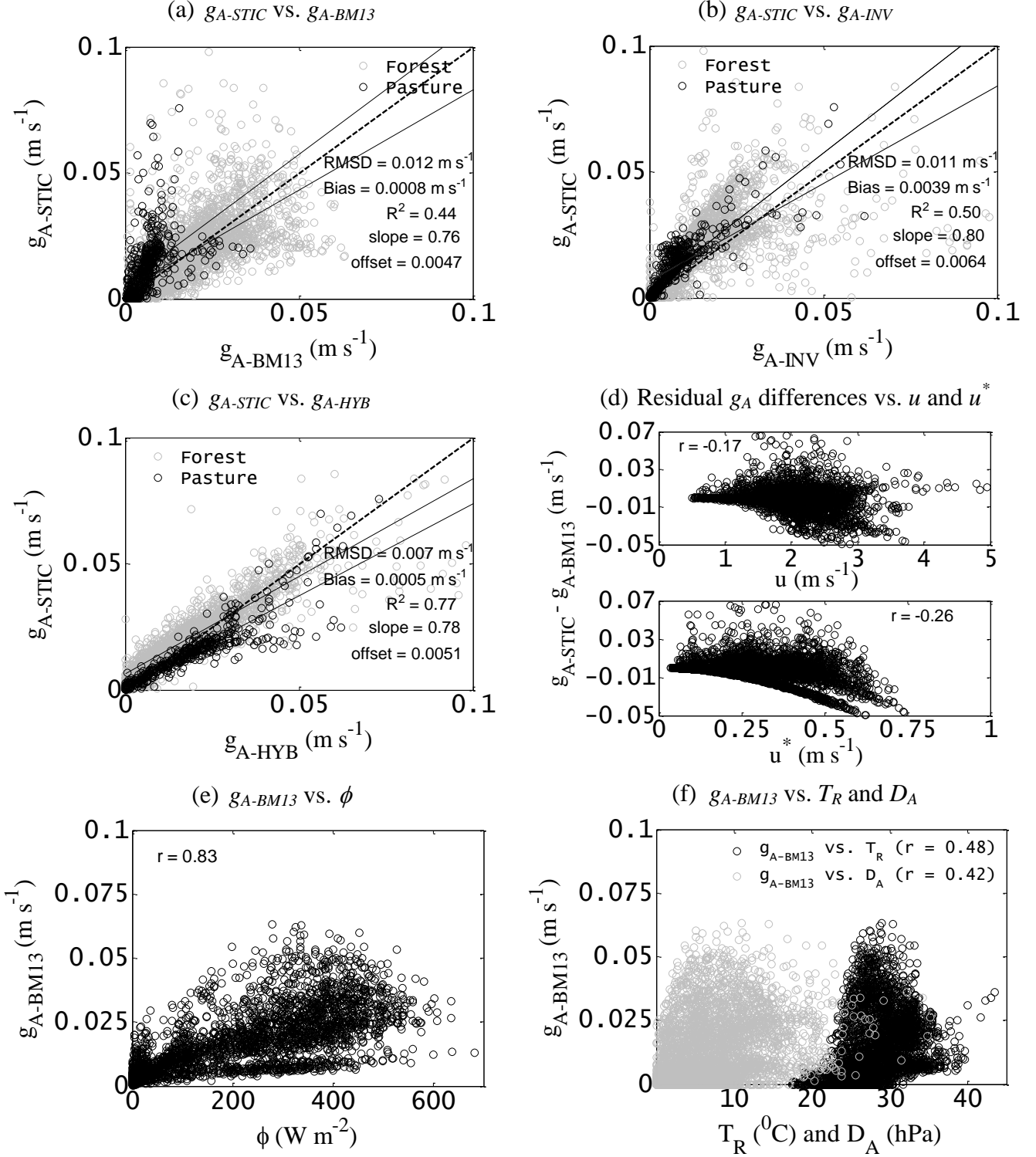


Figure 3. (a) comparison between STIC derived g_C (g_{C-STIC}) and g_C computed by inverting the PM model (g_{C-INV}) over the LBA EC sites, where g_{A-BM13} was used as aerodynamic input in conjunction with tower measurements of λE , radiation and meteorological variables, (b) Residual g_C differences versus wind speed (u) and friction velocity (u^*) over the LBA EC sites.

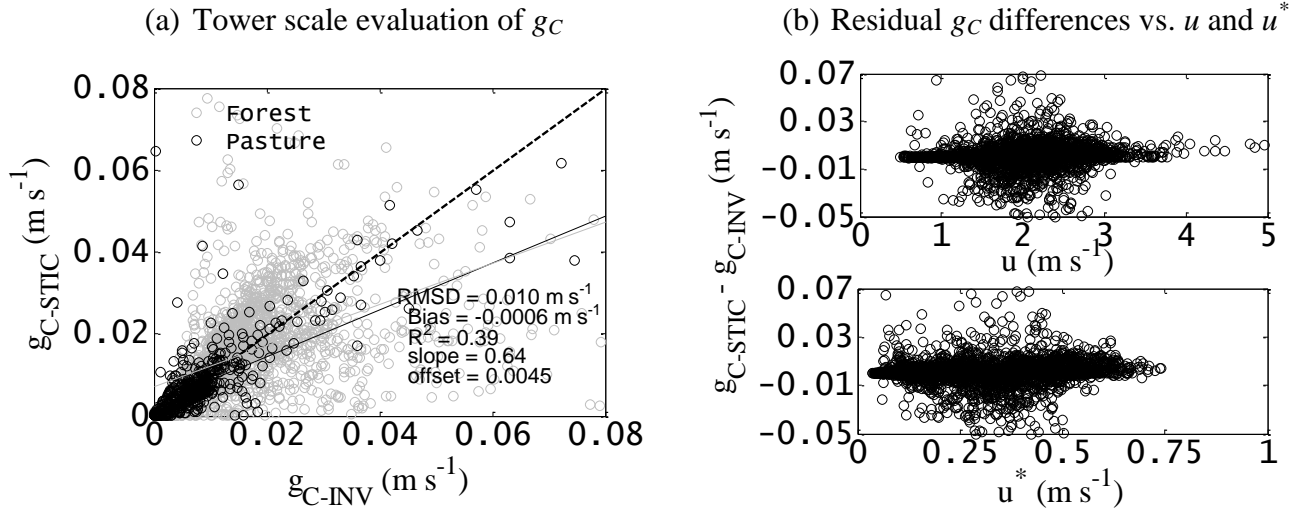


Figure 4. Comparison between STIC derived (a) λE and (b) H over four different PFTs in the Amazon Basin (LBA tower sites). MAPD is the percent error defined as the mean-absolute-deviation between predicted and observed variable divided by mean observed variable.

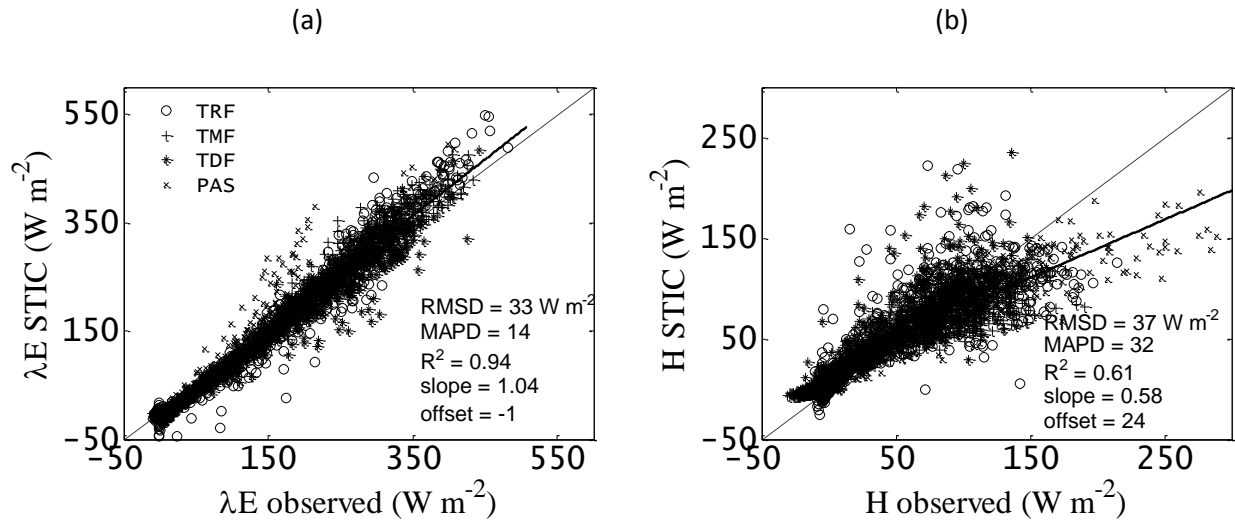


Figure 5. Correlation of coupling ($1-\Omega$) with (a) transpiration (λE_T) and (b) evaporation (λE_E) and over four different PFTs by combining data for all the years, only during dry seasons for all the years, and during drought year 2005. Data for 2005 was not available for TDF and PAS. (c) to (e) Examples of diurnal pattern of Ω (black lines), λE_E (grey dotted lines) and λE_T (grey solid lines) estimated over two ecohydrologically contrasting biomes (K34 for forest and FNS for pasture) in the Amazon Basin (LBA tower sites) during wet and dry seasons.

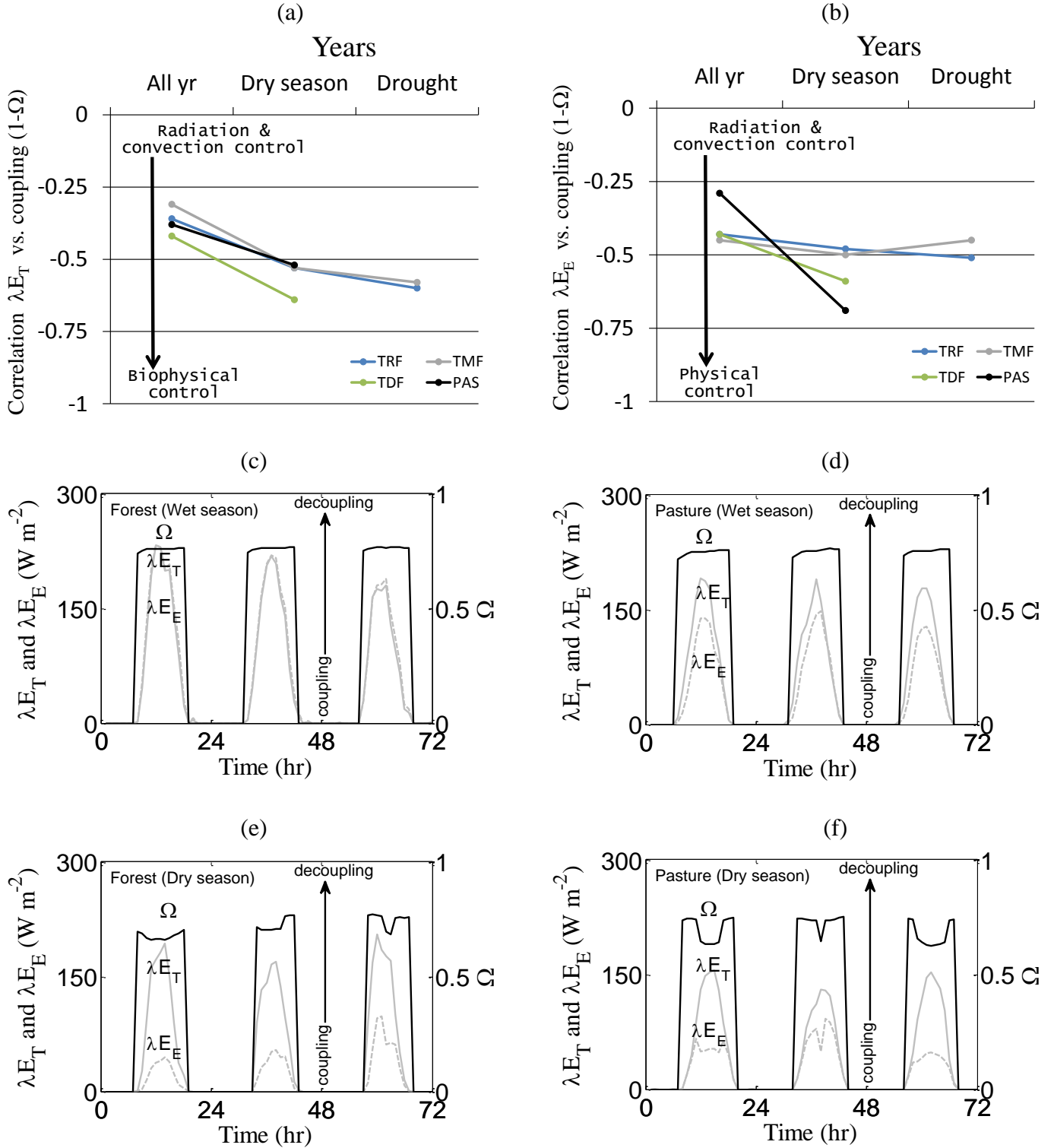
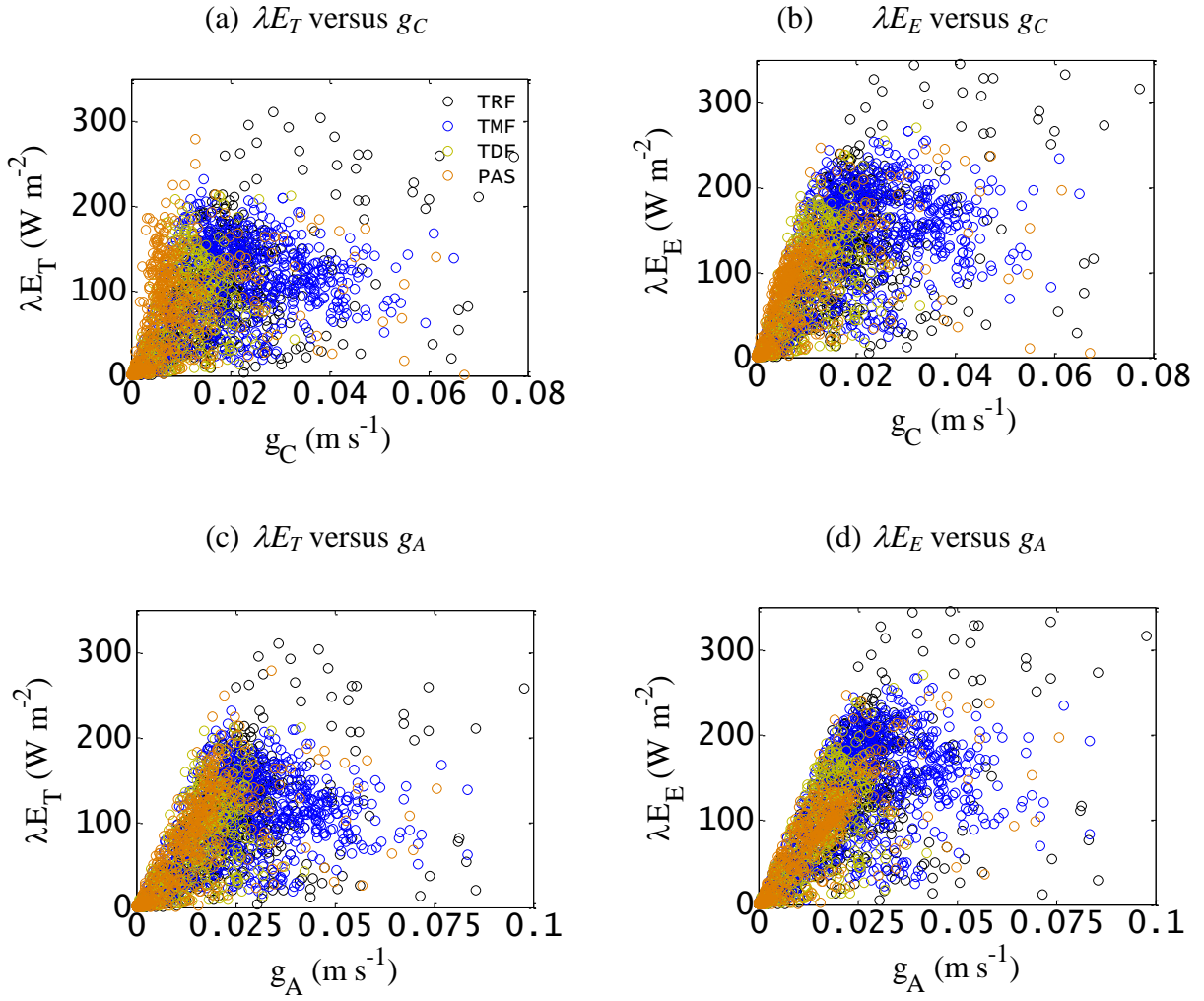


Figure 6. Scatter plots of transpiration (λE_T) and evaporation (λE_E) versus g_C and g_A over four different PFTs in the Amazon Basin (LBA tower sites).



1892 **Figure 7.** Illustrative examples of the occurrence of diurnal hysteresis of transpiration (λE_T) during
1893 wet and dry seasons with canopy and environmental controls over two different sites with different
1894 annual rainfall (2329 mm and 1597 mm, respectively) in the Amazon Basin (LBA tower sites K34
1895 and FNS).

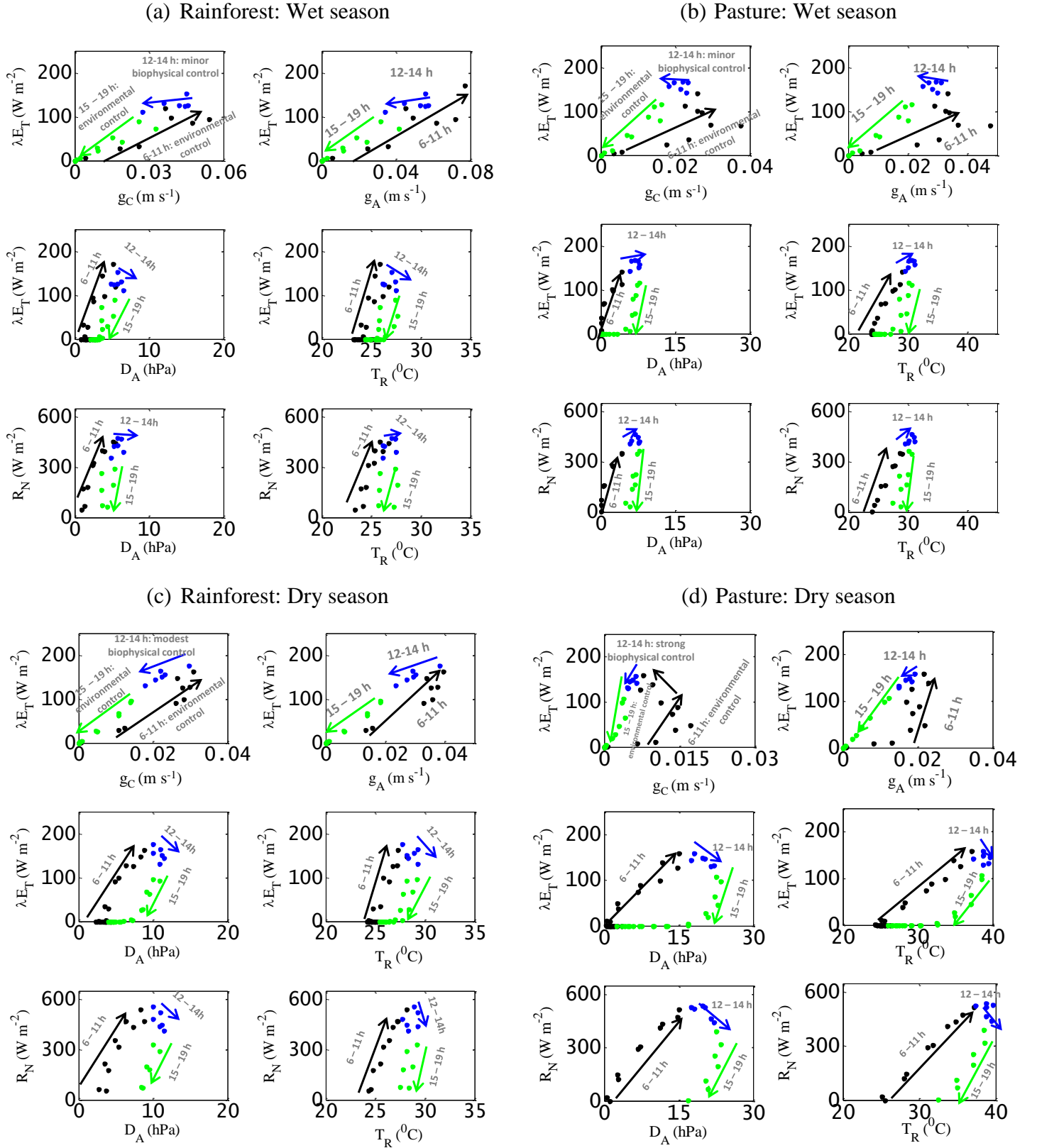
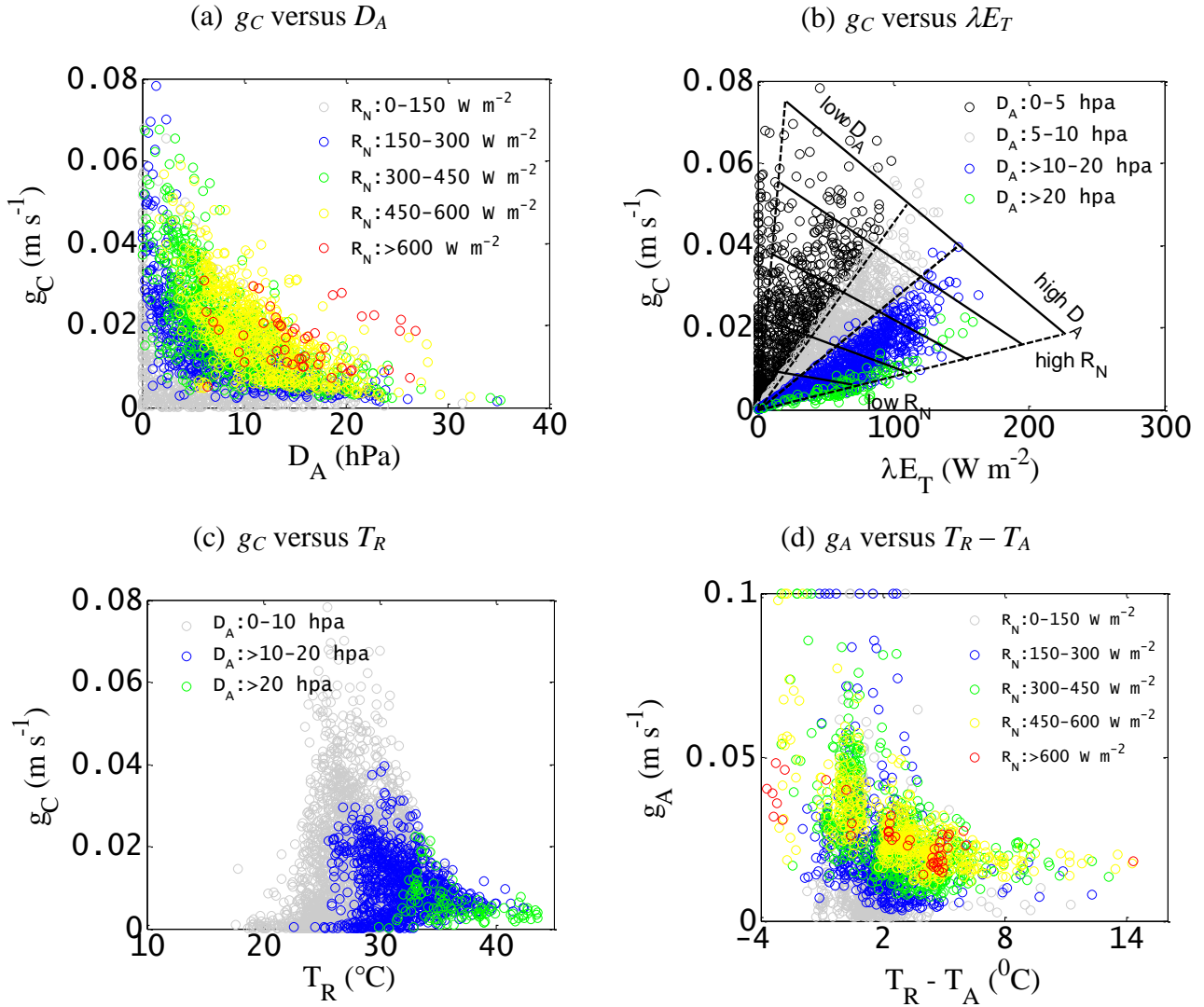


Figure 8. (a) Response of retrieved g_C to atmospheric vapor pressure deficit (D_A) for different classes of net radiation (R_N), (b) Response of retrieved g_C to transpiration for different classes of D_A , (c) Response of retrieved g_C to radiometric surface temperature (T_R) for different classes D_A , (d) Relationship between retrieved g_A and radiometric surface temperature and air temperature difference ($T_R - T_A$) in the Amazon Basin (LBA tower sites).



1909 **Figure 9.** (a) Scatter plots between source-sink height (or in-canopy) vapor pressure deficit (D_0) and
 1910 atmospheric vapor pressure deficit (D_A) for two different classes of g_C/g_A ratios over four PFTs, which
 1911 clearly depicts a strong coupling between D_0 and D_A for low g_C/g_A ratios. (b) Histogram distribution of
 1912 g_C/g_A ratios over the four PFTs in the Amazon Basin (LBA tower sites). (c) Scatter plots between
 1913 g_C/g_A ratio versus surface air temperature difference ($T_R - T_A$) for the four PFT during wet season and
 1914 dry season in the Amazon Basin (LBA tower sites).

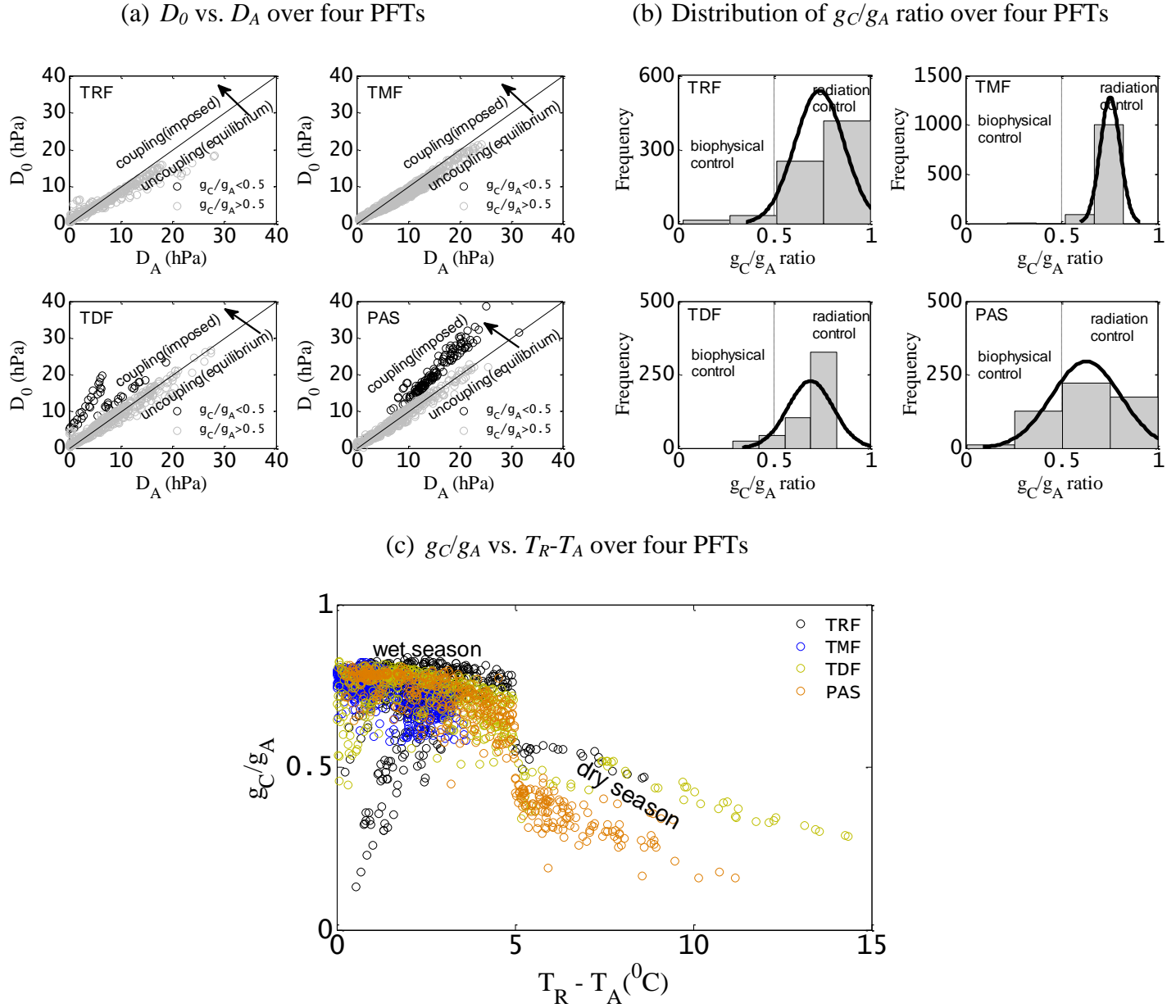


Table A1: Differences in the modeling philosophy of source/sink height vapor pressures (e_0, e_0^*) and dewpoint temperature (T_{SD}), surface wetness (M), and α between STIC1.0, STIC1.1 and STIC1.2.

<u>Variable estimation</u>	<u>Principles</u>		
	<u>STIC1.0</u> (Mallick et al., 2014)	<u>STIC1.1</u> (Mallick et al., 2015)	<u>STIC1.2</u> (This study [Mallick et al., 2016])
<u>Saturation vapor pressure at source/sink height (e_0^*)</u>	e_0^* was approximated as the saturation vapor pressure at T_{R_2} .	Same as STIC1.0	e_0^* is estimated through numerical iteration by inverting the aerodynamic equation of λE (as described in appendix A2). $e_0^* = e_A + \left[\frac{\gamma \lambda E (g_A + g_C)}{\rho c_P g_A g_C} \right]$
<u>Actual vapor pressure at source/sink height (e_0)</u>	e_0 was empirically estimated from M based on the assumption that the vapor pressure at the source/sink height ranges between extreme wet-dry surface conditions.	Same as STIC1.0	e_0 is estimated as $e_0 = e_0^* - D_0$, where D_0 was iteratively estimated by combining PM with Shuttleworth-Wallace approximation (as described in appendix A2). $D_0 = D_A + \left[\frac{\{s\phi - (s + \gamma)\lambda E\}}{\rho c_P g_A} \right]$
<u>Dewpoint temperature at source/sink height (T_{SD})</u>	$T_{SD} = \frac{(e_S^* - e_A) - s_3 T_R + s_1 T_D}{(s_1 - s_3)}$ s_1 and s_3 are the slopes of saturation vapor pressures at temperatures, approximated at T_D and T_{R_2} respectively.	Same as STIC1.0	T_{SD} is estimated through numerical iteration by inverting the aerodynamic equation of λE (as described in appendix A2). $T_{SD} = T_D + \frac{\gamma \lambda E}{\rho c_P g_A s_1}$
<u>Surface moisture availability (M)</u>	As a stand-alone equation, without any feedback to λE .	Same as STIC1.0	A feedback of M into λE is introduced and M is iteratively estimated after estimating T_{SD} (as described in appendix A2).
<u>Priestley-Taylor parameter (α)</u>	As fixed parameter (1.26).	A physical equation of α is derived as a function of the conductances and α is numerically estimated as a variable.	A physical equation of α is derived as a function of the conductances and α is numerically estimated as a variable (eqn. A15) (as described in appendix A2).

1928
1929

Table A2: Fundamental differences in the modeling principles between STIC1.2 and previous approaches for characterising the biophysical controls on λE components.

<u>Biophysical states</u>	<u>Modeling principles</u>	
	<u>Parametric modeling</u> (Ma et al., 2015; Chen et al., 2011; Kumagai et al., 2004)	<u>STIC1.2</u>
g_A	<p>Either g_A is assumed to be the momentum conductance (g_M) or estimated as a sum of g_M and quasilaminar boundary-layer conductance (g_B).</p> $1/g_A = 1/g_M + 1/g_B$ $g_M = u^*/u$ $g_B = f\{Nusselt\ number, leaf\ dimension, thermal\ conductivity\ of\ air\ in\ boundary\ layer, u, kinematic\ viscosity, Reynolds\ number\}$ <p>If u^* is available from EC tower, it is directly used, otherwise u^* is parametrized using Monin-Obukhov Similarity Theory (MOST).</p> <p>Disadvantages: (1) MOST is only valid for an extended, uniform, and flat surface (Foken, 2006). MOST tends to fail over rough surfaces due to breakdown of the similarity relationships for heat and water vapor transfer in the roughness sub-layer, which results in an underestimation of the 'true' g_A by a factor 1-3 (Thom et al., 1975; Chen and Schwerdtfeger, 1988; Simpson et al., 1998; Holwerda et al., 2012). (2) In the state-of-art λE modeling, the parametric g_A sub-models are stand alone and empirical, and do not provide any feedback to g_C, aerodynamic temperature (T_0), and aerodynamic vapor pressures (e_0 and D_0). (3) Additional challenges in grid-scale or spatial-scale g_A estimation are the requirements of numerous site specific parameters (e.g., vegetation height, measurement height, vegetation roughness, leaf size, soil roughness) and coefficients needed to correct the atmospheric stability conditions (Raupach, 1998).</p>	<p>Analytically retrieved by solving 'n' state equations and 'n' unknowns, with explicit convective feedback and without any wind speed (u) information.</p> <p>In a hallmark paper by Choudhury and Monteith (1986), it is clearly stated that 'aerodynamic conductance determined by wind speed and roughness is assumed to be unaffected by buoyancy. Strictly, the aerodynamic conductance should be replaced by a term which accounts for radiative as well as convective heat transfer'. The role of g_A is associated with the role of convection (Choudhury and Monteith, 1986) according to the surface energy balance principle as reflected in the derivation of eqn. (A4). Wind is generated as a result of the differences in atmospheric pressure which is a result of uneven surface radiative heating. Therefore, the aerodynamic conductance (and wind as well) is an effect of net radiative heating and there should be a physical relationship between these two.</p> <p>Advantages: (1) STIC1.2 consists of a feedback describing the relationship between T_R and λE, coupled with canopy-atmosphere components relating λE to T_0 and e_0. (2) Supports the findings of Villani et al. (2003) which stated that during unstable surface layer conditions the major source of net available energy is located at the canopy top and drives the convective motion in the layers above.</p>
g_C	<p>a) If λE measurements are available from the EC towers, g_C is estimated by inverting the PM equation. None of these approaches allow independent quantification of biophysical controls of λE as g_C is constrained by λE itself.</p> <p>(b) Sometimes g_C is modelled either by coupled leaf-scale photosynthesis models (Ball et al., 1987; Leuning, 1995) or g_C is estimated from standalone empirical models (Jarvis, 1976)</p>	<p>Analytically retrieved by solving 'n' state equations and 'n' unknowns where physical feedbacks of g_A, soil moisture, and vapor pressure deficit are embedded (as explained in STIC1.2 equations in Appendix).</p>

1930

Figure A1. Schematic representation of one-dimensional description of STIC1.2. In STIC1.2, a feedback is established between the surface layer evaporative fluxes and source/sink height mixing and coupling, and the connection is shown in dotted arrows between e_0 , e_0^* , g_A , g_C , and λE . Here, r_A and r_C are the aerodynamic and canopy (or surface in case of partial vegetation cover) resistances, g_A and g_C are the aerodynamic and canopy conductances (reciprocal of resistances), e_s^* is the saturation vapor pressure of the surface, e_0^* is the saturation vapor pressure at the source/sink height, T_0 is the source/sink height temperature (i.e. aerodynamic temperature) that is responsible for transferring the sensible heat (H), e_0 is the source/sink height vapor pressure, e_s is the vapor pressure at the surface, z_0 is the roughness length, T_R is the radiometric surface temperature, T_{SD} is the source/sink height dewpoint temperature, M is the surface moisture availability or evaporation coefficient, R_N and G are net radiation and ground heat flux, T_A , e_A , and D_A are temperature, vapor pressure, and vapor pressure deficit at the reference height (z_R), λE is the latent heat flux, H is the sensible heat flux, respectively.

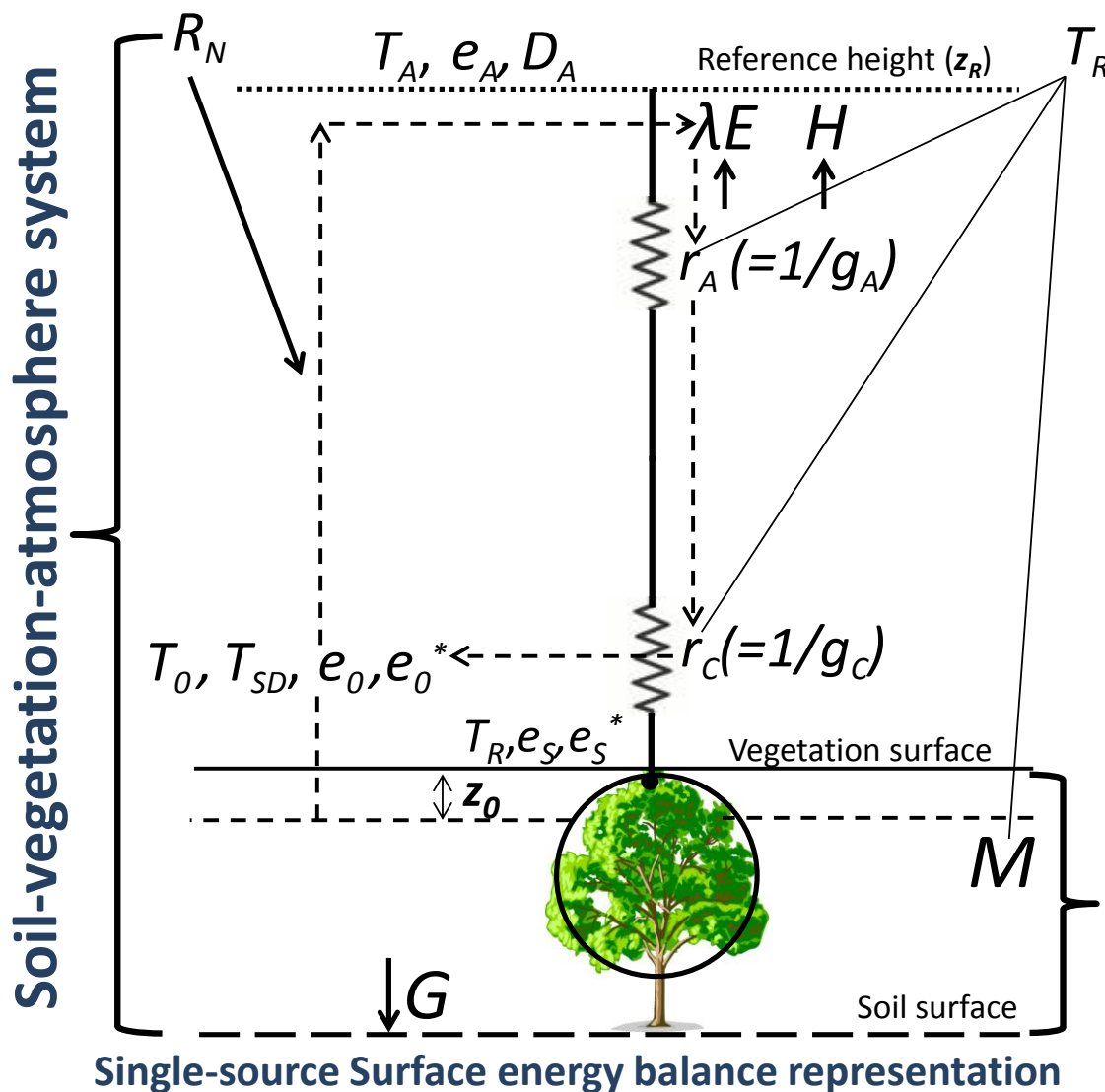


Figure A2. Aerodynamic temperature obtained from STIC1.2 (T_{0-STIC}) versus radiometric surface temperature (T_R) over two different biomes in the Amazon basin. The regression equation of line of best fit is $T_{0-STIC} = 0.67(\pm 0.10)T_R + 10.59 (\pm 2.79)$ with $r = 0.65$.

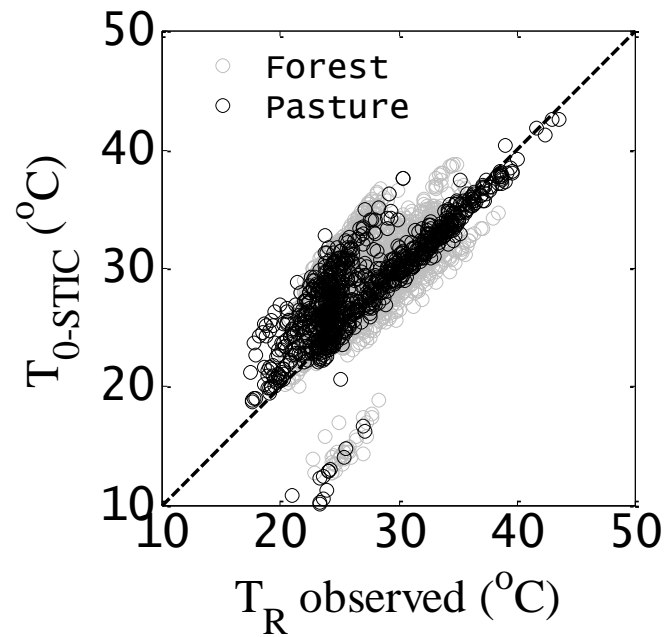


Figure A3. (a) Convergence of the iteration method for retrieving the source/sink height (or in-canopy) vapor pressures (e_0 and D_0) and Priestley-Taylor coefficient (α). (b) Convergence of the iteration method for retrieving the surface wetness (M) and source/sink height dewpoint temperature (T_{SD}). The initial values of λE , g_A , g_C , and T_0 were determined with $\alpha = 1.26$. The process is then iterated by updating λE , e_0 , D_0 , M , T_{SD} , and α in subsequent iterations with the previous estimates of g_A , g_C , and T_0 .

